Nano Research
2021, 14(9): 3159–3173

ISSN 1998-0124 CN 11-5974/O4
https://doi.org/10.1007/s12274-021-3425-9

Review Article

Confined nanospace pyrolysis: A versatile strategy to create hollow structured porous carbons

Rui-Ping Zhang, Wen-Cui Li, Guang-Ping Hao, and An-Hui Lu (✉)

State Key Laboratory of Fine Chemicals, School of Chemical Engineering, Dalian University of Technology, Dalian 116024, China

Received: 31 December 2020 / **Revised:** 24 February 2021 / **Accepted:** 26 February 2021

ABSTRACT

Confined nanospace pyrolysis (CNP) has attracted increasing attention as a general strategy to prepare task-specific hollow structured porous carbons (HSPCs) in the past decade. The unique advantages of the CNP strategy include its outstanding ability in control of the monodispersity, porosity and internal cavity of HSPCs. As a consequence, the obtained HSPCs perform exceptionally well in applications where a high dispersibility and tailored cavity are particularly required, such as drug delivery, energy storage, catalysis and so on. In this review, the fundamentals of the CNP strategy and its advances in structural alternation is first summarized, then typical applications are discussed by exemplifying specific synthesis examples. In addition, this review offers insights into future developments for advanced task-specific hollow structured porous materials prepared by the CNP strategy.

KEYWORDS

confined nanospace pyrolysis, hollow structures, carbon materials, core-shell structures, dispersibility

1 Introduction

Hollow structured porous materials including carbon-based and metal-based composite matters commonly own a porous shell and hollow interior, which have wide applications in energy storage and conversion [1–5], catalysis [6–9], water and air purification [10], and drug delivery [11–15]. Hollow structured porous carbons (HSPCs), as one important branch of HSPMs, have attracted special attentions owing to their structural features in terms of high surface area, large cavity, tunable porosity and controllable particle size, in the past decades. Great efforts have been devoted to developing more controllable synthesis strategies and exploring the task-specific applications. Conventionally, the synthesis mainly relies on templating strategies such as hard, soft, and combined templating method or templating-free strategy. In a templating synthesis, both an interior sacrificial template, e.g., silica, polymer, metals, oxides and micelles etc., and the outer coated polymers as carbon precursors are involved. The hollow spaces are created upon the removal of the interior templates. In the templating-free strategy, it is usually performed by directly carbonizing some hollow-structured carbon precursors such as etched hollow metal organic framework (MOF) precursors or polymers. As a straightforward method, however, these strategies suffer with severe agglomeration during thermal treatment at high temperature, thus resulting in poor dispersion and failing to form stable colloid of the fabricated HSPCs. Moreover, high temperature treatment can cause the structure collapse, destroying the cavity and pore structure. These limitations lead to technical difficulties in the precise design of HSPCs, and restrict its performance in the potential applications.

To solve this bottleneck issue, a "confined nanospace pyrolysis (CNP)" strategy was proposed by Lu's group around a decade ago [16]. Since then, the CNP method has been extensively explored and widely proven to be a general method to create defined HSPCs. The development of the CNP method was inspired by the life practice of removing the shell of a hard-boiled egg (Fig. 1). Analogously, the CNP strategy involves creating a protection shell ("egg shell") on the outer surface of a polymer sphere ("egg") before thermal treatment ("boiling"). By doing so, direct contact between polymer spheres can be avoided, in which the outer silica shell acts as a barrier to prevent the agglomeration during high-temperature treatment. Figure 1 illustrates the difference between the CNP strategy and the conventional direct pyrolysis method. Notably, in CNP strategy, the internal cavity of the HSPCs is *in situ* formed, and can be fine-tuned, which is distinct from the mechanism on creating cavity by templating in conventional methods. Meanwhile, the CNP strategy shows great flexibility in combining with other strategies such as selective etching/dissolution, chemical vapor deposition etc., which enables additional functions in the obtained HSPCs.

In recent years, several reviews on preparing HSPCs have been reported, while mostly focusing on the conventional direct pyrolysis methods with the assistance of the templates [17–21]. However, the CNP strategy, as a newly emerging alternative has not been documented yet. This motivated us to organize this work to overview the latest progress on CNP strategy, mainly including on the construction of HSPCs with intriguing morphologies and various hollow structures (e.g. single shell, double shell, yolk-shell, multi-cavity, hollow fiber, yolk-shell-fiber, hollow polyhedron, etc.), and summarizes their relevant applications, including the fields of energy, catalysis and biomedicine. To begin this journey, recent development of HSPCs promoted by CNP strategy is discussed, by involving

Address correspondence to anhuilu@dlut.edu.cn

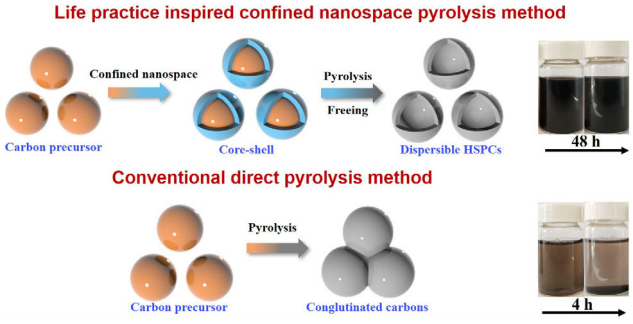

Figure 1 The comparison of the confined nanospace pyrolysis strategy and conventional direct pyrolysis method.

the control of dispersibility, the interior cavity, as well as the extension of morphology and composition of HSPCs from spherical to non-spherical, from single component to multi-components etc. Followingly, the CNP strategy is proven applicable for the designed synthesis of other metal-based hollow structures which are discussed as well. At last, we closed up the review with a prospective regarding further research trends on CNP as well as more advanced HSPCs.

2 Fundamentals of the CNP strategy

The CNP strategy enables exceptional ability in control of the product's monodispersity, the precise alternation of the interior cavity and the fine regulating of the HSPCs' porosity. The mechanism of preventing the aggregation of HSPCs during high-temperature pyrolysis lies in the presence of the protection shell [16]. Also, the coassembly of silicate oligomer species and phenolic resin works nicely for this goal [22]. How to design strong interaction between the carbon precursor surface and silica is particularly important. The coassembly of inorganic and organic phases is based on the Stöber method, which usually relies on solution chemistry involving the hydrolysis and condensation of tetraethyl orthosilicates (TEOS). In this process, the high interface energy and the interface interaction (e.g., hydrogen bond, electrostatic interaction) between the colloidal polymer spheres and silica oligomers can induce the uniform growth of silica shell at the surface of polymer nanospheres. For example, the hetero-charged polymer attracts silanol ($Si\text{-}(OH)_4$) and further condenses into polymer@silica core-shell structure [23]; or the polymer and silanol with the same charge could also assemble in the presence of ionic surfactants such as cetyltrimethylammonium bromide (CTAB) as bridges [24]. It is the vital guiding principle to achieve heterogeneous nucleation on the core and fabricate monodispersed polymer@SiO_2 nanospheres with a certain silica thickness. As for the adjustment of the thickness of silica shells, the following equations can be used

$$M_{polymer} = 4/3 \cdot \pi r_1^3 \cdot N \cdot \rho_1 \quad (1)$$

$$M_{SiO_2} = (4/3 \cdot \pi r_2^3 - 4/3 \cdot \pi r_1^3) \cdot N \cdot \rho_2 \quad (2)$$

According to the given shape parameters before and after adjustment, the amount of TEOS precursor required can be calculated concretely. Therefore, the thickness of the silica layer can be precisely controlled. In the CNP method, the outer silica confined layer can prevent the contact between adjacent particles, so the particle coagulation can be eliminated and the obtained HSPCs exhibit in a dispersible state.

The origin of the internal cavity is controlled by the self-activation process. The nature of the self-activation is pressure driven volume expansion and the accompanying chemical deposition. During pyrolysis of a polymer nanosphere confined in a silica nanoreactor, volatile carbonaceous species are deposited in or inside the hermetical silica shell to form a layer of carbon/silica hybrid shell, and the polymer spheres transform into carbon cores accompanied by volume shrinkage, thus resulting in the hollow spaces. At the same time, the volatile gases enrich in the cavity to build up the pressure, which further enlarge of the hollow spaces.

The development of the porosity in the HSPC's shells is essentially relevant to the *in situ* chemical etching process by the generated gases, e.g., CO_2, H_2O (the widely used activation agents), during self-activation. The gases are difficult to penetrate through the hermetical silica shells and enriches in the cavity to build up the pressure. The state equation for ideal gases ($pV = nRT$) can theoretically estimate the pressure generated by CO_2 and other gases released in the cavity, which is above 630 atm. CO_2 and H_2O partially gasify the carbon framework under such a high pressure, creating enlarged porosity. The reaction equations are as follows

$$CO_2(g) + C \rightarrow 2CO(g) \quad (3)$$

$$H_2O(g) + C \rightarrow CO(g) + H_2(g) \quad (4)$$

In addition, through regulating the thickness of confined layer or the openness of pores in silica shell, the control of confined degree and internal gas pressure can be achieved. And then, the *in-situ* dynamic evolution of the porosity in the shells, the control of cavity size, or even the morphologic transformation from hollow to yolk-shell structure can be reached.

3 Advances of the CNP strategy and relevant HSPCs

Based on the CNP strategy, the construction of HSPCs is capable of achieving several unique features. In this section, we discuss the recent advances of CNP strategy in control of the product's monodispersity, the precise alternation of the interior cavity, the fine regulating of the porosity and the extension to non-sphere and composite structures.

3.1 Control of monodispersity against high-temperature sintering

Monodispersity is one of the most important properties of HSPCs in many practical applications such as drug carriers, colloidal catalysts, absorbents for aqueous solution, and inks. Conventionally, they suffer from condensing and agglomeration during high-temperature pyrolysis process. To resolve this critical issue, in 2011, Lu's group proposed the CNP strategy to synthesize discrete and highly dispersible hollow carbon spheres (HCS) with tailorable shell thickness and cavity size [16]. Polystyrene nanospheres, phenolic resin and silica were served as cavity template, carbon precursor and confined shell, respectively (Fig. 2(a)). During the high-temperature pyrolysis of the dual-shell structured PS@PF@SiO_2 nanospheres, the silica shell acted as a hard cover can prevent polymer/carbon from agglomeration. Afterwards, silica shell was removed by NaOH etching, obtaining the discrete, water dispersible HSPCs (Figs. 2(b)–2(e)). Zeta potentials result indicated that they could be dispersed in aqueous solution stably in the pH range between 5–13 where the absolute value of zeta potentials was higher than 30 mV (Fig. 2(f)). The dispersed solution had no sign of aggregated precipitation over 48 hours, as shown by the optical photograph (Fig. 2(g)). In contrast, the carbon nanospheres from direct pyrolysis of PS@PF was not dispersible in water, in turn confirming the advantage of CNP strategy.

Table 1 Key structural parameters of hollow structured porous carbons fabricated through the CNP method

Structure	Precursor for the core	Template	Particle size (nm)	Cavity size (nm)[a]	Pore structure; S_{BET} ($m^2 \cdot g^{-1}$)[b]	Ref.
Hollow	Phenolic resin	Polystyrene	100–440	38–310	Microporous; 603.8	[16]
Solid	Polybenzoxazine	Fe_2O_3	90	Fe_2O_3 core: 40	Microporous; 502	[25]
Solid, rough surface	Polybenzoxazine	—	150	—	Mesoporous; 562–711	[26]
Hollow	2, 4-Dihydroxybenzoic acid and formaldehyde	Oleic acid	—	40–160	Mesoporous; 787	[27]
Multi-cavity	Polybenzoxazine	Glycerol trioleate	100	10–105	Mesoporous; 571–761	[33]
Hollow	3-Aminophenol and formaldehyde	—	160	120	Mesoporous; 342–783	[28]
Hollow	Polyacrylonitrile	Polystyrene	200	110–350	Mesoporous; 955	[29]
Hollow	Polyacrylonitrile	Polystyrene	410	260–350	Micro/mesoporous; 546	[30]
Hollow/Double shell	Polystyrene	—	410	300–430	Mesoporous; 29–1,392	[31]
Yolk-shell	Resorcinol and formaldehyde	—	190	Cavity: 150; yolk: 61–93	Ordered mesoporous; 1068	[34]
Yolk-shell	$AgNO_3$, resorcinol and formaldehyde	—	700	Cavity: 550; yolk: 400	Mesoporous; 440	[36]
Yolk-shell	Polybenzoxazine	—	410	Cavity: 290; yolk: 220	Mesoporous; 626–1,038	[37]
Yolk-shell	Resorcinol and formaldehyde	—	400	Cavity: 0–350; yolk: 250–360	Mesoporous; 300–616	[38]
Hollow/Yolk-shell	Resorcinol and formaldehyde	—	300; 400	Hollow to yolk-shell	Mesoporous; 507–1,425	[39]
Hollow/Yolk-shell	Resorcinol and formaldehyde	—	Rod: 150; sphere: 420	Rod (cavity: 90; yolk: 10) Sphere (cavity: 300; yolk: 170)	Rod: 722 Sphere: 982	[40]
Yolk-shell	Resorcinol and formaldehyde	—	680–920	—	Mesoporous; 543–703	[41]
Solid	Phenolic resin	F127	100	Pore size: 3.1–10 nm	Order mesoporous; 1,186	[49]
Solid	Polybenzoxazine	F127	170	Pore size: 3.1–10.7 nm	Ordered mesoporous; 840	[50]
Solid	Polybenzoxazine	F127	40	—	Mesoporous; 1,050	[51]
Hollow	Resorcinol and formaldehyde	—	110	40	Mesoporous; 809	[52]
Hollow	Zn,Co-ZIF	—	120	—	Mesoporous; 809	[53]
Hollow	ZIF-8	—	260	145	Mesoporous; 667–1,086	[54]
Hollow	Polydopamine	β-FeOOH nanorod	72	18	Mesoporous; 210	[55]
Solid	Carbonate	—	900	—	Mesoporous; 129	[56]
Solid	$ZnSn(OH)_6$	—	60	—	Mesoporous; 112	[57]
Hollow	FeOOH	MoO_3 nanorods	200	—	Mesoporous; 103	[58]

[a]Cavity size: applicable for the hollowed structures. For others, a separate description is given; [b]S_{BET}: The specific surface area is calculated by using Brunauer–Emmett–Teller (BET) method.

Additionally, the outer diameter, cavity size, and shell thickness could be precisely tailored when adopted CNP method. Furthermore, additional functions can be imparted on the basis of the CNP strategy. For example, the discrete magnetic Fe_3O_4@C nanoparticles were prepared by confining Fe_2O_3@Polymer in a hermetical silica shell to achieve good dispersibility in blood environment [25].

Other than the *in-situ* coating of silica through the hydrolysis and condensation of TEOS, the pre-synthesized silica nanoparticles could also be used as seeds for follow-up assembling into a core-shell structure via electrostatic interaction. Recently, Wang et al. reported a charge-driven, interfacial assembly method to synthesize carbon nanospheres (CNSs) with controlled surface roughness and excellent water dispersibility (Fig. 2(h)) [26]. The positively charged polybenzoxazine-based polymer nanospheres (PNSs) were mixed with the negatively charged commercial silica nanoparticles in the pH range of 2.1–4.5, leading to colloidal coagulation and the formation of PNS@SiO_2 core-shell nanospheres. Due to the decomposition of polymer parts and the chemical vapor deposition of volatile carbonaceous species among silica nanoparticles during the pyrolysis process, the surface roughness created which exhibited good dispersibility. In addition, the roughness of CNSs could be adjusted by tuning pyrolysis temperature and the amount of colloidal silica.

3.2 Precise control of the cavity structures

Apart from the good dispersibility properties, the construction and tune of interior hollow structure can also be realized by employing the CNP method. Owing to the extensive development of synthesis methods in recent years, various HSPCs have been synthesized, which show entire hollow structure, yolk-shell structure, multi-yolk structure, and multi-shell structure [11]. Among them, the entire hollow and yolk-shell structures are the vital foundation in the tall building of HSPCs, which can be fabricated by combining with different synthesis strategies, such as melting impregnation, selective etching/dissolution, or nanocasting, etc. Therefore, from the perspective of entire hollow and yolk-shell structures, this section reviews the preparation and control of cavity promoted by the CNP method.

3.2.1 *Entire hollow carbon spheres*

CNP strategy can be used to enlarge and tune the original cavity by self-activation mechanism. Sun et al. fabricated hollow

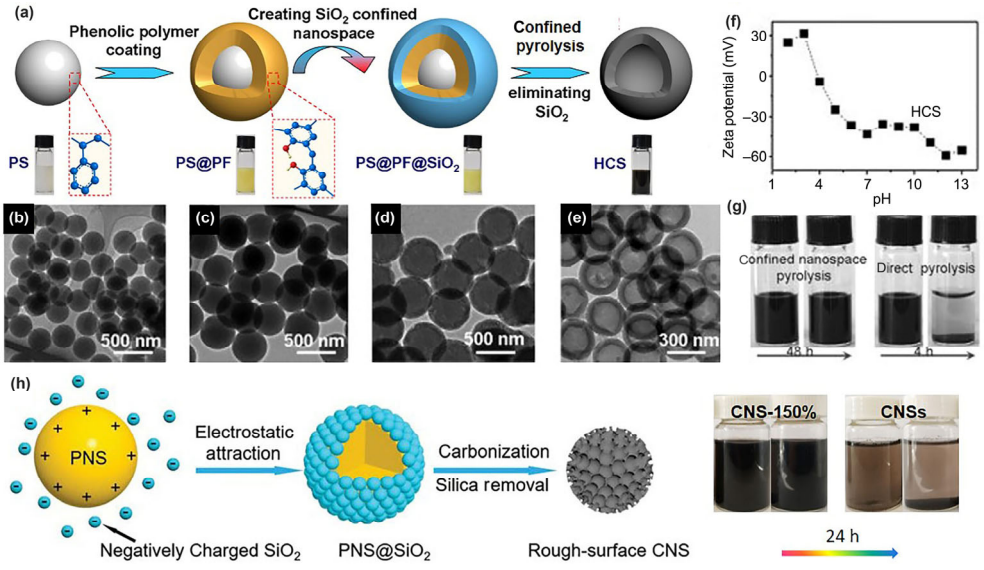

Figure 2 (a) Schematic illustration for the synthesis of hollow carbon nanospheres by confined nanospace pyrolysis, insets show photographs of the stable aqueous suspensions of each product; TEM images of (b) PS, (c) PS@PF, (d) PS@PF@SiO_2, (e) HCS. (f) Zeta potentials of HCS in aqueous solution in pH range of 2–13. (g) Photographs of the HCSs dispersed solution derived from confined nanospace pyrolysis and direct pyrolysis. (h) Synthesis process of PNS@SiO_2 and rough-surface CNSs via surface-charge driven method. (a)–(g) Reproduced with permission from Ref. [16], © WILEY-VCH Verlag GmbH & Co. KGaA, Weinheim 2011. (h) Reproduced with permission from Ref. [26], © WILEY-VCH Verlag GmbH & Co. KGaA, Weinheim 2019.

carbon spheres (HCSs) and observed the phenomenon of cavity expansion by pyrolyzing the silica confined hollow polymer spheres [27]. During the carbonization, the cavity expanded with different degree by changing the openness of silica shell (Fig. 3(a)). In Route 1, hollow polymer nanospheres were directly pyrolyzed and the diameter of cavity was about 55 nm. When the pyrolysis process was confined in the silica shell, the obtained HCS-2@SiO_2 exhibited an enlarged cavity with a diameter of ~ 160 nm (Route 2). In order to open the mesopores of HPS@SiO_2 by removing the CTAB template, this sample was refluxed in ethanol in the presence of hydrochloride acid. After carbonization, the obtained HCS-3@mSiO_2 (mSiO_2 represents SiO_2 with opened mesopores) showed a smaller cavity with a diameter about 120 nm compared to that of HCS-2@SiO_2 (Route 3). The cavity expansion mechanism can be described in Fig. 3(b). During pyrolysis process, *in situ* generated gases (CO_2, H_2O, etc.) gathered in the hollow space to build up high pressure and partially gasified the carbon shell by the self-activation mechanism, eventually increasing the porosity and the hollow space. In reverse, the removal of *in-situ* generated gases by continuous evacuation decreases the self-activation effect, leading to smaller size than HCS-2@SiO_2. (Route 4).

During pyrolysis, cavities can also be generated *in-situ*. Yang et al. adopted mesoporous polymeric nanospheres as carbon precursors, and the solid core was transformed into hollow structure during pyrolysis [28]. The synthesis procedure is illustrated in Fig. 4. Microemulsions were firstly formed in the mixture of ethanol and water, and then 3-aminophenol/formaldehyde (APF) resin polymerized on the surface of micelles to form resol-micelle complex. After hydrothermal treatment, APF resin nanospheres with internal mesoporous structure were obtained. Direct pyrolysis of the polymer spheres resulted in solid carbon spheres with internal mesopores (Route A). However, transferring from solid aminophenol formaldehyde polymer resins to hollow mesoporous carbon spheres was discovered through a CNP process by Route B, that's probably because the highly porous interior carbon framework was more easily to be etched by pyrolysis gases compared with the outer compact carbon shell. Inversely, in Rout C, silica sphere was used as sacrificial core material, and APF resin as polymer shell. Compared with Route A and C, the confined space constructed by Route B can generate enlarged mesoporous and cavity during pyrolysis. While the other two samples prepared via Route A and C without confined nanospace exhibit a solid and microporous structure. CNP method is a general strategy, and different types of polymer spheres can be used as carbon precursors. For example, Du et al. chose core-shell structured polystyrene@polyacrylonitrile (PSPAN) spheres as carbon precursor for the synthesis of N-doped

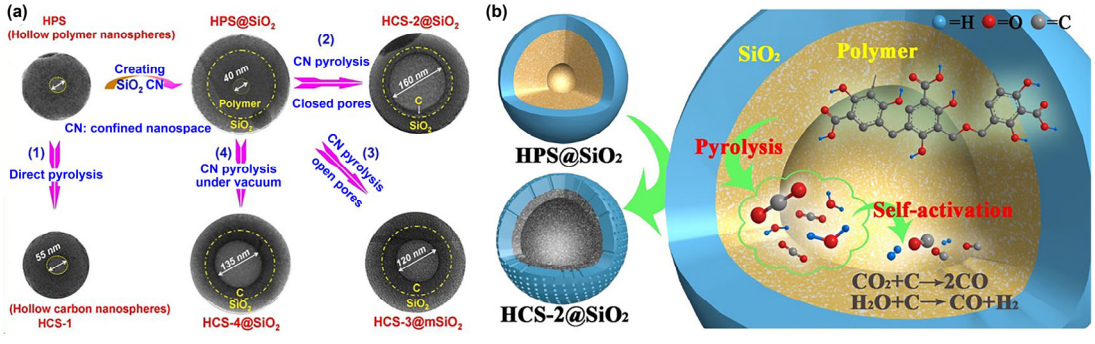

Figure 3 (a) The synthesis processes of hollow carbon nanospheres. (b) Fabrication scheme for the self-disposition and hollow core expansion inside the silica layer nanoreactor. (a) and (b) Reproduced with permission from Ref. [27], © WILEY-VCH Verlag GmbH & Co. KGaA, Weinheim 2013.

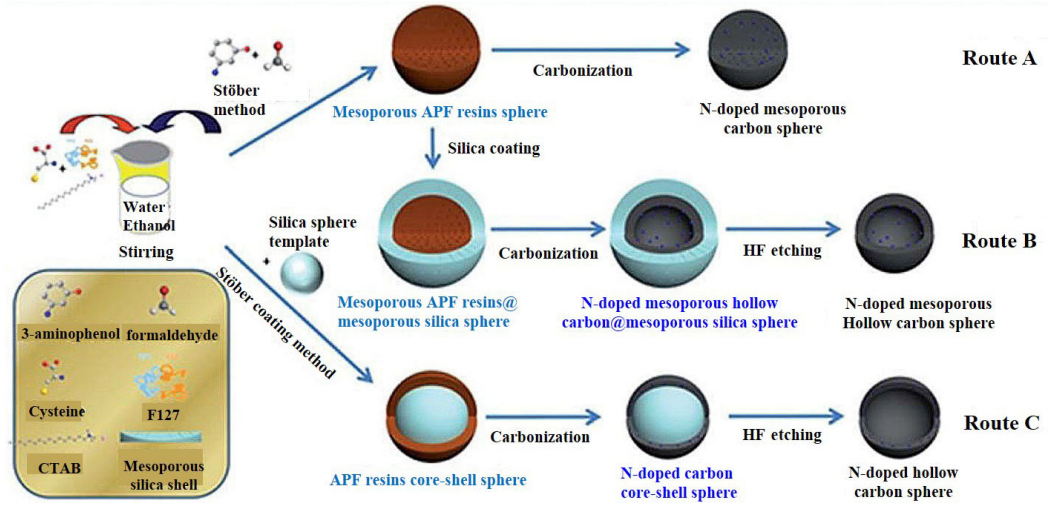

Figure 4 Synthesis routes of N-doped carbon spheres with different nanostructures, Route A: N-doped mesoporous carbon nanospheres (N-MCNSs) via direct pyrolysis, Route B: N-doped mesoporous hollow carbon nanospheres (N-MHCNSs) via outer-silica-assisted coating method, Route C: N-doped hollow carbon nanospheres (N-HCNSs) via traditional template method. Reproduced with permission from Ref. [28], © The Royal Society of Chemistry 2014.

HSPCs with a tunable diameter and cavity by using the CNP strategy [29].

The pore openness degree of silica shell has great effect on the development of the hollow structures. For example, Du et al. used PSPAN spheres as carbon precursors that were coated with a silica layer having different openness degree [30]. After pyrolysis and silica removal process, N-doped hollow carbon spheres (denoted as N-HCS-*x*, where *x* represents the different degree of openness for the confined condition including open (O), semi-open (S) and compact (C)) were obtained (Fig. 5(a)). Directly pyrolysis of PSPAN led to severe agglomeration and the obtained samples displayed an irregular structure (Route 1). In Route 2, a layer of silica was the bridging agent and TEOS as silica source, followed by CTAB removal process to obtain PSPAN@SiO_2 nanospheres with open pores of silica shell (denoted as PSPAN@SiO_2-O). In Route 3, when CTAB remained in silica shell, the environment was more closed (semi-open condition, denoted as PSPAN@SiO_2-S). When PSPAN cores were coated by a compact silica layer without adding CTAB (using TPOES as silica source), PSPAN@SiO_2-C was obtained (Route 4). TEM images of N-HCS-*x* represented all the three samples that exhibited a clear hollow structure, but the thickness of carbon shell was apparently different (Figs. 5(b)–5(d)). With the openness degree of silica shell decreasing, the carbon shell thickness of the N-HCS-*x* increased. The reason was that more compact silica shell led to comparatively more carbon residue deposition during pyrolysis of PSPAN due to the gases were difficult to penetrate through the silica layer. It is worth mentioning that, polystyrene (PS) spheres itself can also be used as carbon precursor in CNP strategy due to the complete decomposition properties of PS upon thermal treatment when temperature is above 300 °C. For example, Chen et al. synthesized PS@SiO_2 spheres with different thickness of silica shell [31]. With the increasing thickness of silica, the structure of the obtained HCSs changed sequentially from a hollow sphere with thin shell to hollow sphere with double thin shells and further to an asymmetric sphere with thicker carbon shells. In the case of thinner silica shell, the volatile carbonaceous species deposited on both the inner and outer surface of the silica shell, resulting in thin shell or double shell. However, a thicker silica shell provided a more compact and robust confined condition, so more carbon species were deposited on the inner surface of the silica shell, resulting in thicker carbon layer, which was in perfect agreement with previous observations [30].

3.2.2 *Multicavity carbon spheres*

Porous carbon materials with multi-cavity are expected to be promising energy storage materials. For, example, Wang et al. reported a surfactant-directed space confined polymerization to synthesize N-doped multichambered carbon (MCC)

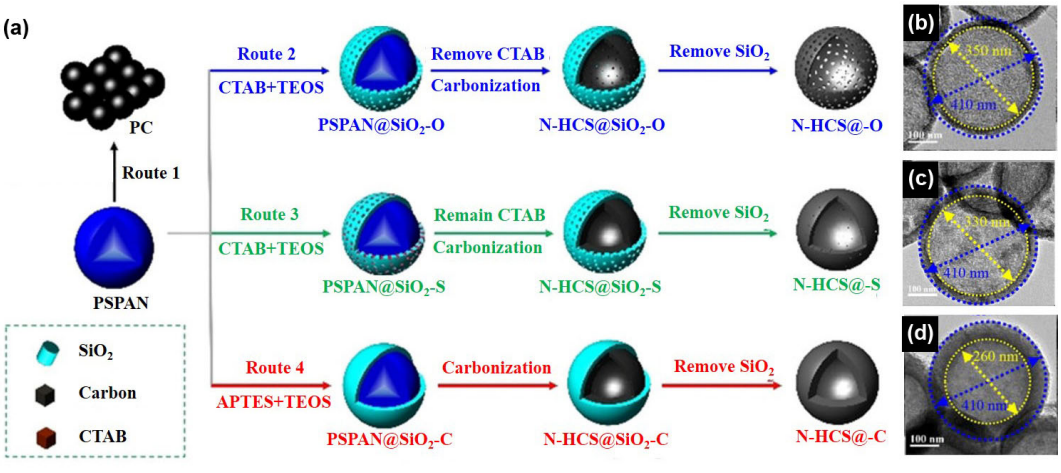

Figure 5 (a) Schematic synthesis of N-HCS samples with different degrees of porosity. TEM images of (b) N-HCS-O, (c) N-HCS-S and (d) N-HCS-C. Reproduced with permission. from Ref. [30], © Wiley-VCH Verlag GmbH & Co. KGaA, Weinheim 2019.

microspheres with microporous shells by a dual-surfactant system consisting of sodium dodecyl benzene sulfonate and triblock copolymer Pluronic F127 [32]. To further develop CNP strategy on such multicavity morphology, Zhang et al. fabricated grid-like multicavity carbon spheres with tunable cavity size combined with "surface free energy-induced assembly" strategy [33]. Porous carbon materials with multi-cavity could promote the adsorption potential in interior space and facilitate the access of guest active species into the cavity. The synthesis process could be mainly divided into two parts: i) synthesis of grid-like multicavity polymer spheres, ii) confined nanospace pyrolysis (Fig. 6(a)). Firstly, the primary nanoemulsions were formed. Subsequently, the resols polymerized around the nanoemulsions to form the sub-structural units, which then tended to form polymer assemblage due to their high surface free energy. After pyrolysis, the obtained sample showed the cavities with enlarged sizes as compared to that of the directly pyrolyzed sample. Moreover, the cavity sizes and numbers were both tunable by changing the sizes of the nanoemulsions, and the size enlargement effect promoted by confined nanospace pyrolysis was again applicable. In these studies, the generation or expansion of the cavities was caused by the confinement effect of silica shell during the pyrolysis, which was the embodiment of the unique feature of this strategy.

The grid-like morphology can also be generated *in-situ* by the direct pyrolysis of mesoporous silica coated polybenzoxazine resin. Yu et al. synthesized the internal gridded hollow carbon spheres with tunable density and microporous shell from solid polymer spheres under regulated pyrolysis micro-environment [34]. By altering the crosslinking degree of polymer spheres and the pyrolysis process conditions, the size and density of carbon-bridge grids can be tuned.

3.2.3 *Yolk-shell structured hollow carbon spheres*

Yolk-shell HCSs, as a kind of rattle-like core-shell structure with a movable core, can also be fabricated by the CNP strategy. For example, Liu et al. reported that yolk-shell carbon nanospheres can be prepared by using mesoporous resorcinol formaldehyde (RF) resin spheres as the carbon precursor on which a layer of silica was coated, followed by pyrolysis and removal of silica with HF solution (Fig. 7) [35]. Interestingly, a phase separation between the silica shell and the carbon core occurred during pyrolysis process. The obtained yolk-shell carbon nanospheres had the sizes of 190 nm in diameter, 21 nm in shell thickness and 60 nm in yolk diameter. The yolk consisted of ordered 2D hexagonal mesoporous structure. The size of diameter and cavity can be controlled by changing the synthetic parameters, such as the thickness of silica layer, concentration of carbon precursor, etc. The thickness of silica shell can be precisely adjusted from 15, 17, 22 to 26 nm with the TEOS amount from 80, 100, 150 to 200 μL along with the total amount of the reaction mixture of 40 mL. In addition, replacing the RF resin by APF resin led to the N-doped carbon shell. Following the abovementioned procedure, similar structure, nitrogen doped yolk-shell carbon nanospheres were obtained.

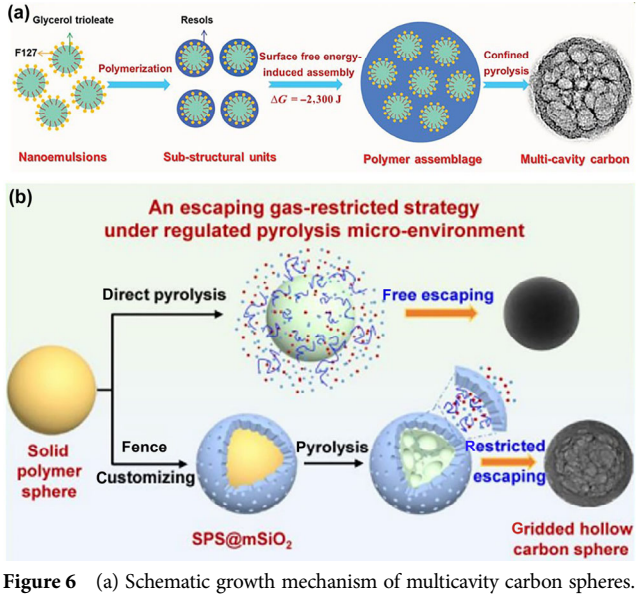

Figure 6 (a) Schematic growth mechanism of multicavity carbon spheres. (b) Illustration of the synthesis of internal gridded hollow carbon spheres. (a) Reproduced with permission from Ref. [33], © WILEY-VCH Verlag GmbH & Co. KGaA, Weinheim 2017. (b) Reproduced with permission from Ref. [34], © Tsinghua University Press and Springer-Verlag GmbH Germany, part of Springer Nature 2021.

By integrating metallic compounds with HCSs, multifunctional HCSs can be prepared. For example, a novel kind of Ag@carbon@meso-SiO_2 nanosphere was prepared by the extended CNP strategy [36]. In the synthesis, a layer of mesoporous silica was coated on AgBr@RF spheres by the self-assembly of cationic surfactants (CTAB) and oligomers of the hydrolyzed silica precursor (TEOS) under basic conditions. Upon pyrolysis in N_2, the yolk-shell structured Ag@carbon@meso-SiO_2 spheres were obtained. Notably, the shrinkage of the polymer layer resulted in a hollow space between the carbon inner shell and the mesoporous silica outer shell. In contrast, the cavity was not formed when AgBr@RF spheres were pyrolyzed directly. As a supplementary, the calcination of the Ag,AgBr@RF@meso-SiO_2 in air led to the formation of the rattle-type Ag,AgBr@meso-SiO_2.

Alternatively, Sun et al. have prepared a unique hollow carbon structure, i.e., mesoporous carbon shell and hollow interior but with microporous carbon core which interlinked with the mesoporous carbon shell, by using the CNP strategy [37]. This is the first synthesis of nanocarbons with such morphology. This synthesis involved the coating of mesoporous silica layer on the surface of polybenzoxazine-based solid polymer spheres (SPS), followed by pyrolysis and silica removal process (Fig. 8(a)). TEM images showed that the core was indeed attached to the shell by rotation around the axis of the holder to +40° and −40° (Fig. 8(b)). The mechanism of cavity formation was also investigated by using thermogravimetry-mass spectrometry (TG-MS). When the pyrolysis process was confined in silica shell, polymer spheres were transformed into the carbon core accompanied by volume shrinkage to form hollow space. And the volatile fragments that were difficult to penetrate through the hermetical silica shells were deposited into the mesopores of silica shell, forming a layer of carbon/silica hybrid

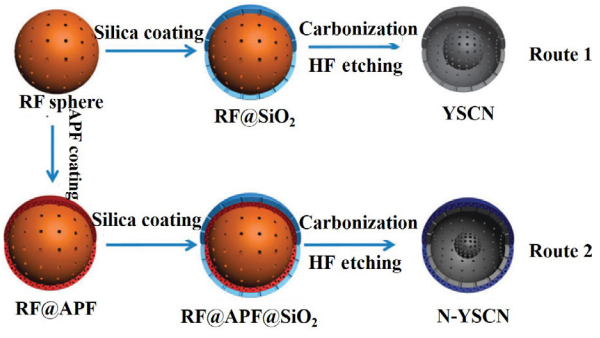

Figure 7 Synthesis scheme of yolk-shell structured carbon nanospheres (YSCNs, Route 1) and N-doped yolk-shell structured carbon nanospheres (N-YSCNs). Reproduced with permission from Ref. [35], © The Royal Society of Chemistry 2015.

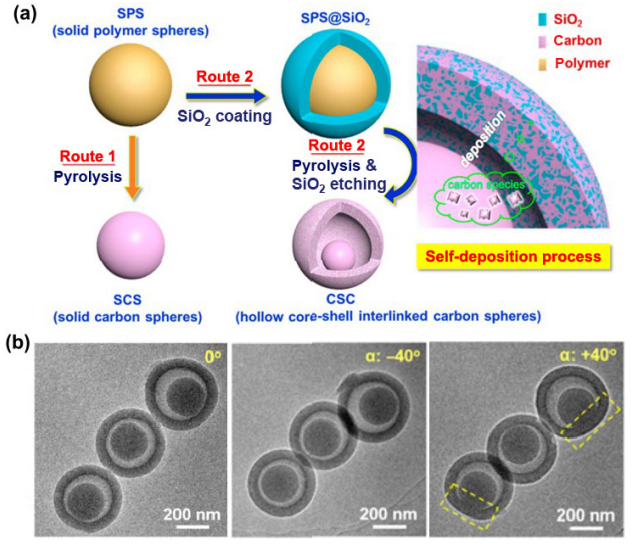

Figure 8 (a) Synthesis route and interface self-disposition scheme for hollow core-shell interlinked carbon spheres (CSC). (b) TEM images of CSC with the sample holder tilted to –40°, 0° and +40° by rotation around the axis of the holder. Reproduced with permission from Ref. [37], © American Chemical Society 2015.

shells. TG-MS curves revealed that the volatile carbonaceous species released from silica coated SPS (SPS@SiO_2) were detected at the temperature greater than 300 °C, which was much higher (~ 200 °C) than that released from SPS.

Similar to the preparation of HSPCs with entire cavity, the confined degree can also affect the hollow structure of the yolk-shell carbon nanospheres based on the CNP strategy. The extent of the confinement was reflected from the pore opening degree and the thickness of silica layer. The pore opening degree of the outer silica shell can be classified into open (O), semi-open (S) and compact (C) as discussed above [29]. For example, Chen's et al. synthesized carbon spheres with different cavity structure and pore size [38]. Firstly, RF resin spheres were synthesized by an extended Stöber method, which were proceeded in four different routes (Fig. 9). When they were pyrolyzed directly, solid carbon spheres were obtained (Route 1). In Route 2, the pyrolysis of RF@SiO_2 nanospheres with open pores of silica shell (RF@SiO_2-O) led to a core-shell structure with solid carbon core and fluffy carbon shell. Most of the volatile carbonaceous species could escape from the open pores and there was not enough pressure to cause obvious shrinkage of the RF core and separation between the core and shell during

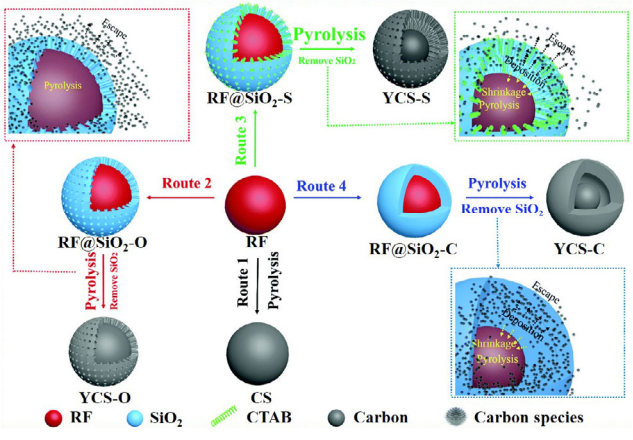

Figure 9 Schematic illustration of the synthesis procedure of YCS under different confined conditions. Reproduced with permission from Ref. [38], © The Royal Society of Chemistry 2019.

the pyrolysis process. Meanwhile, part of carbonaceous species was deposited in the pores of the silica shell. After removal of silica, the fluffy carbon shell was formed. When CTAB remained in silica shell, the environment is largely closed (semi-open condition), and the carbon core shrunk obviously as the evolved gases *in situ* activated the carbon core (Route 3). The obtained the yolk-shell structured carbons exhibited a clear yolk-shell structure with outer diameter of 400 nm and core diameter of 250 nm. In the absence of CTAB in the coating process, the formed silica shell was nonporous. Thus, the obtained material exhibits yolk-shell structure with a thinner and more compact porous carbon shell (Route 4).

Apart from the openness degree of silica shell, the thickness of silica shell was another parameter that reflected the degree of confined conditions. Chen et al. further investigated the effect of the silica thickness on the structure development of the carbon spheres by pyrolyzing compact silica-coated RF resin spheres [39]. Varied thickness of silica layer can lead to different structures after confined nanospace pyrolysis. When RF spheres were pyrolyzed directly without confined conditions, solid carbon spheres (CSs) were obtained. In contrast, pyrolysis in a compact silica shell led to cavity formation. Thinner silica shell resulted in a less compact condition, in which some pyrolysis gas would remain in the confined space to create a cavity and some pyrolysis gas ran out of the silica shell, to form the hollow mesoporous structure. Thicker silica shell led to a compact condition, in which the RF resin sphere would be transformed into the inner core and some part of the pyrolysis gas was deposited on the inside surface of silica shell, forming a yolk-shell mesoporous structure. The polymerization degree of RF spheres can also affect the hollow structure. RF spheres treated with hydrothermal process (increasing the polymerization degree) were pyrolyzed under the same confined conditions, and as a result solid carbon sphere with a diameter of ~ 300 nm was obtained. Clearly, versatile yolk-shell carbon nanospheres can be synthesized following the CNP strategy by changing the confined degree, precursor type, the porous structure of the silica shell etc.

The outer silica shell can also be fabricated by one-pot synthesis method, in which the hydrolysis-condensation of TEOS and polycondensation of RF occurred in the same solution to form a nanocomposite with the core/shell architecture. Taking TEOS/RF system as an example, the hydrolysis and condensation rate of TEOS and the polymerization rate of RF could be tuned by changing ethanol–water volume ratios, the amount of surfactant, the temperature, etc. It would generate various core-shell structures and shapes including RF@SiO_2/RF, SiO_2@SiO_2/RF and so on. After pyrolysis, different structures of hollow hybrid carbon/silica spheres were obtained, and the HSPCs were finally synthesized after silica removal. The one-pot method was facile and time-saving. Zhang et al. synthesized carbon spheres and silica spheres with different hollow structures via one-pot method by tuning ethanol–water volume ratios (4:24, 8:20, 12:16), followed by pyrolysis and different post treatments (Fig. 10) [40]. The polymer–silica–surfactant (PSS) composites were firstly fabricated by the co-sol–gel process of RF precursor and TEOS in the presence of CTAB which acted as bridging agent between negatively charged RF resin and SiO_2 oligomers. When the ethanol–water volume ratio was 4:24, rod-like PSS composites with RF as cores and interpenetrated RF/silica hybrids as shell could be obtained. During pyrolysis process, the inner RF cores transformed to carbonaceous counterpart and shrank greatly, giving rise to cavity between the cores and shells, causing the formation of rattle-type tube structure with inner carbon cores and outer carbon/silica shell (Route 1). After removal of silica, rattle-type carbon tubes

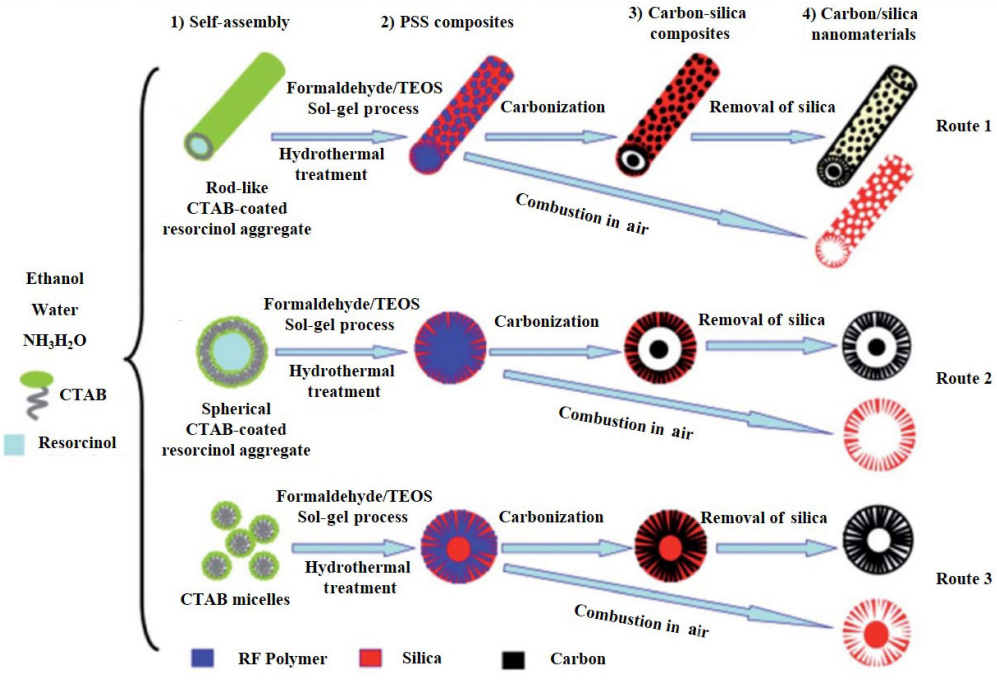

Figure 10 Schematic demonstration for the synthesis of polymer-silica-surfactant composites and mesoporous carbon/silica nanomaterials by one-pot sol–gel approach in an ethanol aqueous solution. Reproduced with permission from Ref. [40], © The Royal Society of Chemistry 2012.

could be obtained (denoted as E4-C), and the complementary product E4-SiO_2 exhibited a rod-like structure with hollow core and silica shell after calcination in air. When the ethanol–water volume ratios were 8:24, the PSS possess a spherical morphology with RF as cores and RF/silica hybrids as shell. After pyrolysis and post treatment, similar with E4-C, rattle-type carbon spheres (E8-C,) and hollow SiO_2 spheres (E8-SiO_2) were obtained (Route 2). When the ethanol–water volume ratio increased to 12:16, the inner cores were silica and the outer shells were hybrids of RF polymer and silica. After pyrolysis and post treatment, E12-C exhibited a hollow structure with mesoporous carbon shell and the structure of E12-SiO_2 was flower-like sphere with solid core and radial mesopores shell (Route 3).

Analogous to the one-pot approach, Qiao et al. reported a silica-assisted method based on the one-pot reaction of TEOS, resorcinol, and formaldehyde in the mixture of water/alcohol/NH_4OH/CTAC for synthesizing the highly monodisperse mesoporous carbon nanospheres [22]. The morphology includes solid, hollow and yolk-shell, which can be controlled by tuning the TEOS amount and the hydrothermal conditions. Wang et al. synthesized yolk-shelled carbon spheres with tunable yolk volume and porosity by controlling the TEOS concentration [41]. The RF-SiO_2 hybrid spheres with inner RF cores and RF/silica hybrid shell can be fabricated via a co-sol-gel process. During pyrolysis, the interior RF gradually shrank, giving rise to the formation of cavity between the carbon cores and C/SiO_2 shell, and after removing SiO_2, yolk-shell carbon spheres were finally achieved. As increasing the concentration of TEOS, the yolk ratio also increased. In contrast, the sample prepared without adding TEOS exhibited a solid sphere morphology, reflecting the impact of TEOS on the structure development. The one-pot method could greatly simplify the synthesis procedure. Nevertheless, compared with the layer-by-layer assembly and coating strategy, there were certain critical shortcomings. The hydrolysis and condensation rates of TEOS and the polymerization rate of RF were hard to simultaneously control under given conditions, so that it was difficult to precisely tune the size of the polymer core as well as the thickness and silica/polymer ratio of the shell.

Thanks to the above achievements, we can envisage that the CNP strategy is highly effective for the manipulation of the hollow structures. The mechanism of cavity formation is distinct from the traditional template methods [42–48]. Using this strategy, the morphology, hollow structure, sizes (including thickness of shell, diameter of hollow space, yolk size, outer size, etc.) and porosity could be adjusted precisely by varying synthesis conditions.

3.3 Precise control of the porosity

The CNP strategy can also be applied to tune the porosity, especially the preparation of ordered mesoporous carbon spheres (O-MCS) with adjustable pore sizes. For example, Du et al. synthesized HSPCs with tunable ordered mesoporous based on the self-activation of mesoporous polymer spheres (Fig. 11(a)) [49]. Due to the *in-situ* volatile gases (e.g., CO_2, H_2O) during the carbonization process, the mesoporous size would be enlarged. For comparison, the directly carbonized sample exhibited smaller size, and no pore enlargement was observed. The mesoporous size of O-MCS could be tuned by changing the amount of TEOS in 100 mL reaction mixture (Fig. 11(b)).

When the amount of TEOS was less than 0.5 mL, confined nanospace pyrolysis has no visible effect on the increase of mesoporous sizes. Further increasing the TEOS amounts (0.5–1.5 mL), the mesoporous sizes of the obtained O-MCS increased from 3.1 to 10 nm. That's because for less TEOS, the silica shell was too thin to confine the volatile gases in the nanospace and could not produce a high pressure to enlarge the mesopores (Fig. 11(c)). In contrast, the high-pressure volatile gases serving as activation agents would etch much more pore walls to expand the mesopores.

In addition, the pore shrinkage of pore could be inhibited by employing this strategy. Zhang et al. reported order mesoporous carbon spheres with enlarged mesopores based on the CNP strategy [50]. The directly pyrolyzed sample showed microporous feature, whose pore size shrank from 2 to 1 nm. While CNP strategy can enlarge the mesoporous size. Importantly, through this synthesis strategy, the mesoporous sizes could be tuned

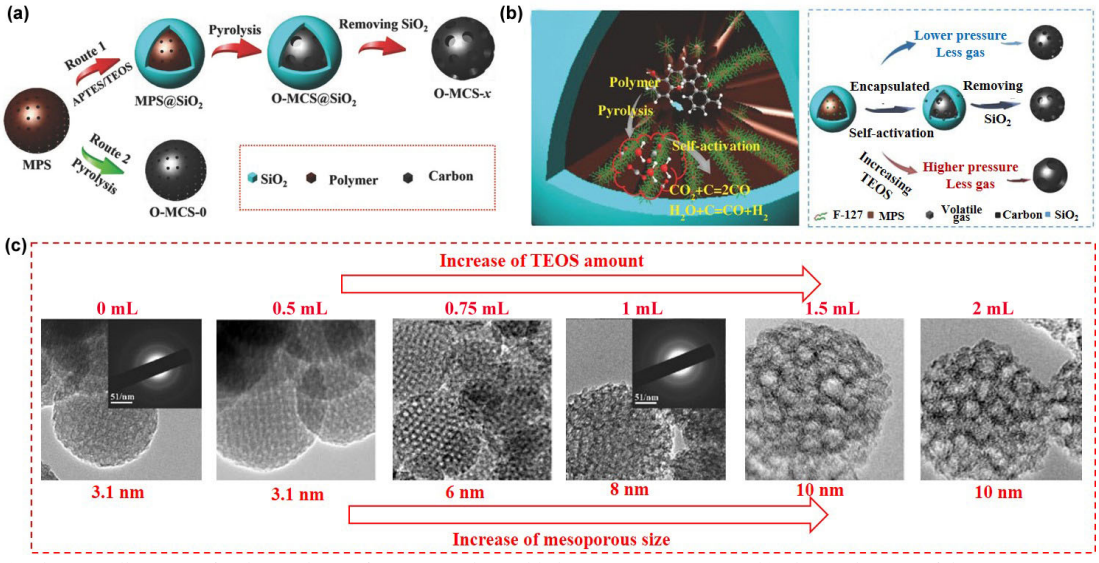

Figure 11 (a) Schematic illustration for the synthesis of O-MCS with tunable large mesoporous size. (b) The mechanism of the mesoporous size expansion inside the compact silica shell. (c) The changing trends of the mesoporous sizes with the increase of TEOS amount (scale bar: 20 nm). Reproduced with permission from Ref. [49], © WILEY-VCH Verlag GmbH & Co. KGaA, Weinheim 2018.

by deliberately changing the thicknesses of silica shells. With the increase of TEOS amount, the mesoporous sizes increased from 3.5 to 10.7 nm, which had a perfect linear relationship between the two variables was established with a high correlation coefficient (R^2) of 0.997.

3.4 The extension of morphology control: From spherical to non-spherical

The CNP strategy is flexible that can be extended from spherical systems to non-spherical even complex structures. For example, Zhang et al. synthesized porous carbon nanofibers with tunable porosity [51]. The synthesis process was illustrated in Fig. 12(a). The uniform polymer nanofibers (PNFs) were firstly fabricated via a controlled hydrothermal approach by using resorcinol and hexamethylene tetramine (HMT) as carbon precursor and Pluronic F127 as the morphology-directing agent. Then a layer of mesostructured silica was coated on the surface of PNFs via the surfactant-templating sol-gel process by using TEOS as silica precursor and CTAB as bridging-agent, followed by removing the CTAB from the silica shell with a hydrochloric acid alcohol solution so that to open the mesopores. During pyrolysis process, the pores were enlarged by self-activation effect and the obtained sample exhibited a core-shell nanocable structure with obvious mesoporous carbon fiber-like cores (Fig. 12(b)). In contrast, the conventional pyrolyzed sample showed a microporous structure (Fig. 12(c)).

The CNP strategy led to the formation of intertwined carbon matrix and SiO_2 in the mesoporous shell. After the removal of SiO_2, the remaining carbon framework is not rigid enough to maintain the mesoporous structure thus the mesopores may shrink, leading to the transformation from mesopores to micropores. Lu and co-workers utilized this pore-shrinkage phenomenon to Li-S battery cathodes. The initially formed mesopores on the shell could facilitate easy infiltration of active materials (sulfur) into the interior and the subsequent narrowed microporous shell (pore size: 0.58 nm) could restrain polysulfide diffusion to prevent "shuttle-effect" [52]. Different from the previous work, the obtained samples exhibited a hollow structure instead of mesoporous carbon core. The reason is that CTAB remained in the silica shell construct a more compact environment, that may lead to a higher pressure promoted by the pyrolysis gas and facilitate the formation of complete hollow structure by the self-activation.

The CNP strategy could also extend to the synthesis of MOF-based derivates. The mechanism of cavity construction is similar to that of polymer-based materials. For example, Liu et al. reported a rigid-interface induced outward contraction

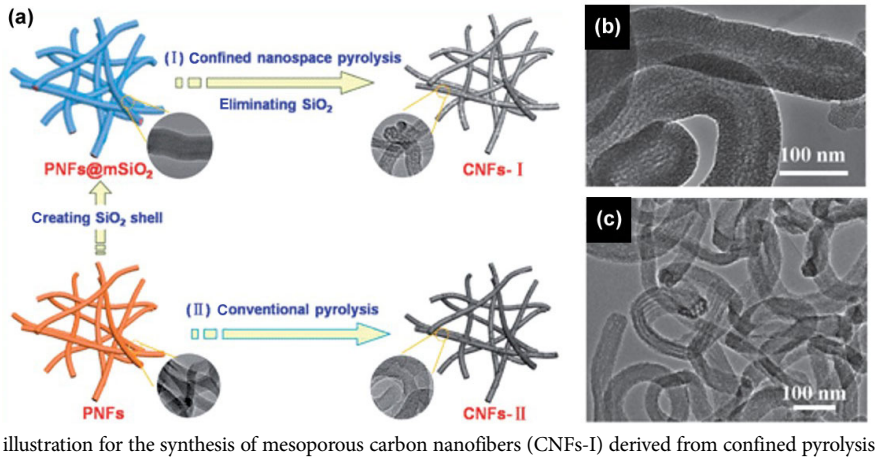

Figure 12 (a) Schematic illustration for the synthesis of mesoporous carbon nanofibers (CNFs-I) derived from confined pyrolysis strategy and microporous carbon nanofibers (CNFs-II) derived from direct pyrolysis; TEM images of (b) CNFs-I and (c) CNFs-II. Reproduced with permission from Ref. [51], © The Royal Society of Chemistry 2013.

process to synthesize hollow mesoporous carbon nanocubes (HMCNCs) through the pyrolysis of $mSiO_2$ coated ZIF-8 nanoparticles, followed by removal of SiO_2 (Fig. 13(a)) [53]. When silica shell was thick, the obtained HMCNCs exhibited a hollow structure with foam-like carbons (Route 1, Figs. 13(b) and 13(c)). In contrast, a solid mesoporous carbon nanocubes was obtained when the silica shell was thinner (Route 2, Figs. 13(d) and 13(e)). The mechanism could be explained as follows. During pyrolysis process, ZIF-8 precursors located at the outmost layer adjacent to $mSiO_2$ were transformed to carbon and migrated into the mesopores of $mSiO_2$ shell. Subsequent pyrolysis of ZIF-8 then occurred preferentially on the preformed carbon embedded within silica. A thicker $mSiO_2$ shell was rigid enough to provide a tensile force to pull the ZIF precursors "outward" during pyrolysis, resulting in the formation of hollow space due to volume reduction of carbonized ZIF-8. However, a thin layer of silica was not sufficient to provide enough driving force, so that the inward shrinkage occurred to form a sunk and solid structure. To verify the pyrolysis process, the sample was polysized at different temperature (400, 500, 600 and 700 °C). With the increase of temperature, hollow structure formed gradually. It was notable that the direct pyrolysis of bare ZIF-8 exhibited a microporous structure without cavity, indicating that silica shell played a critical role in the formation of mesopores and hollow space.

This method can also overcome the problem of agglomeration and irreversible fusion of the nanoparticles during pyrolysis. For example, Zhang and co-workers reported a mesoporous-silica ($mSiO_2$)-protected calcination strategy to prevent aggregation under high-temperature pyrolysis conditions [54]. Firstly, the MOF core, Zn,Co-ZIF was synthesized following the synthesis of ZIF-8, except that Zn^{2+} was partially substituted by Co^{2+}. Subsequently, a mesoporous SiO_2 shell was coated on the surface of Zn,Co-ZIF dodecahedra by using TEOS as silica precursor and CTAB as pore directing template, thus to form Zn,Co-ZIF@$mSiO_2$ nanoparticles. After pyrolysis, Co,N co-doped carbon framework (Co,N-CNF) with interior hollow cavity which possess porous skeletal structure was obtained. For comparison, the experiment of direct pyrolysis of Co,N-CNF was carried out and the obtained sample aggregated severely, which indicated that $mSiO_2$ shell play a vital role in preventing the aggregation during high-temperature pyrolysis process. In addition, the specific surface area and cumulative pore volume of Co,N-CNF were 1,170 $m^2 \cdot g^{-1}$ and 1.52 $cm^3 \cdot g^{-1}$, which were much higher than that of the direct pyrolysis sample (540 $m^2 \cdot g^{-1}$ and 0.46 $cm^3 \cdot g^{-1}$).

3.5 The extension of composition: From polymers to other composite materials

The hollow structured metal/carbon nanocomposites could be another product by employing CNP strategy. Transition metal oxides have become the research hotspot due to their promising applications in intelligent control, catalysis, energy storage and conversion, and fuel cells. And the coating of metallic nanoparticles with porous carbon materials could prevent the nanoparticles from aggregation and corrosion under harsh chemical conditions owing to the excellent chemical stability of the carbon protecting shells. On the other hand, the combination with carbon shell can alleviate the volume change in the charge storage process and improve the conductivity. Lei and coworkers reported a synthesis of coaxial Fe_3O_4@C hollow particles with a rice-grain morphology via this strategy [55]. The fabrication process was illustrated in Fig. 13(f). The rod-shaped akagenite (β-FeOOH) nanoparticles were first coated with polydopamine and silica successively. Under the confined pyrolysis environment created by polydopamine and silica shells, the gas molecules (CO, H_2O, H_2, etc.), arising from the

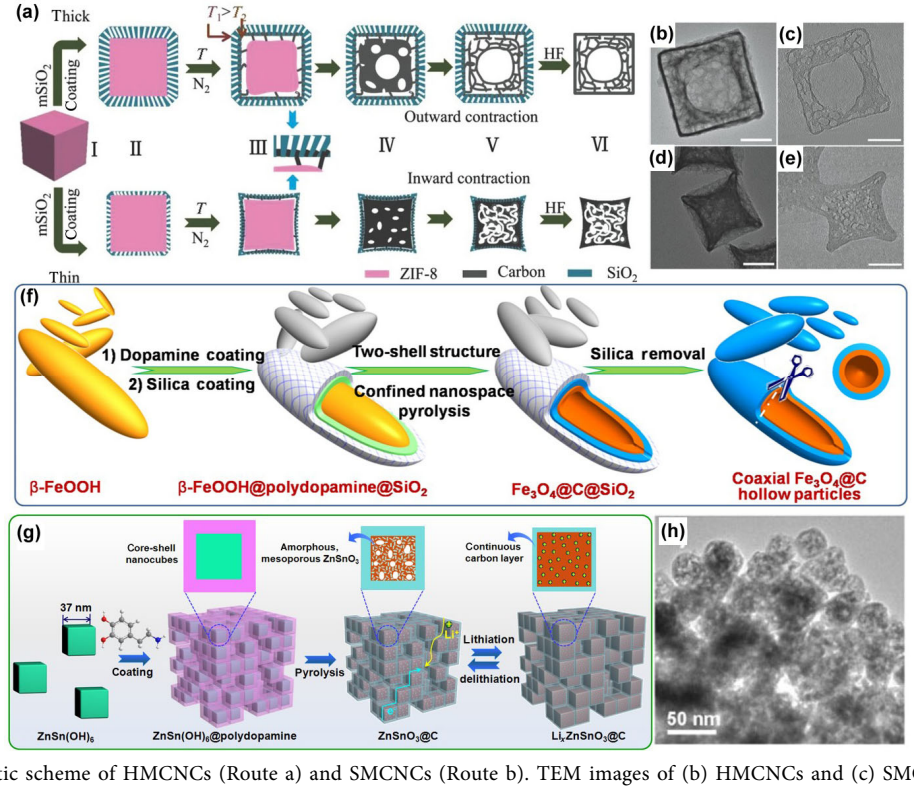

Figure 13 (a) Synthetic scheme of HMCNCs (Route a) and SMCNCs (Route b). TEM images of (b) HMCNCs and (c) SMCNCs. ET slices of (d) HMCNCs and (e) SMCNCs. (f) Schematic illustration for the synthesis of coaxial Fe_3O_4@C hollow particles with a penetrated mesochannel. (g) Synthetic scheme of mesoporous $ZnSnO_3$@C nanocubes. (h) TEM images of $ZnSnO_3$@C. (a)–(e) Reproduced with permission from Ref. [53], © WILEY-VCH Verlag GmbH & Co. KGaA, Weinheim 2017. (f) Reproduced with permission from Ref. [55], © WILEY-VCH Verlag GmbH & Co. KGaA, Weinheim 2013. (g) and (h) Reproduced with permission from Ref. [56], © WILEY-VCH Verlag GmbH & Co. KGaA, Weinheim 2014.

pyrolysis of the polydopamine and dehydration of β-FeOOH, would generate a large pressure to facilitate the formation of cavity. After etching silica, the coaxial Fe_3O_4@C hollow particles were finally obtained.

In addition to SiO_2, polymer shells (e.g., polydopamine) can also act as confined layers to fabricate mesoporous metal@C core-shell structure. In order to fabricate mesopores, carbonate or hydroxyl oxide were employed as metallic core. As an example, Han et al. synthesized bimetal oxide $ZnSnO_3$@C nanocubes with well-developed interior mesoporous $ZnSnO_3$ core and a continuous thin carbon layer by pyrolyzing the core-shell structured $ZnSn(OH)_6$@polydopamine hybrid (Fig. 13(g) [56]. During pyrolysis, $ZnSn(OH)_6$ was decomposed into $ZnSnO_3$ nanoparticles and the escape of water molecules created mesopores in the interior space, thus to form the mesoporous $ZnSnO_3$@C nanoparticles with a carbon thickness of about 5 nm (Fig. 13(h)). It is worth noting that the specific surface area and pore size of $ZnSnO_3$@C were higher compared with pure $ZnSnO_3$ due to the confinement effect of the carbon coating process. Such a mesoporous structure can better accommodate the mechanical strains caused by volumetric changes during charge/discharge cycles. Similarly, Fe_3O_4@C nanotubes with a hierarchically porous structure can also be fabricated by using same polydopamine-coated method [57]. Firstly, a layer of uniform FeOOH shell was coated on the surface of rod-like MoO_3 template, followed by removal of the template to obtain FeOOH nanotubes. Then, the obtained FeOOH nanotubes were coated with a thin and continuous layer of polydopamine. During pyrolysis, mesopores between Fe_3O_4 nanoparticles were created due to thermal dehydroxylation of the FeOOH and polydopamine was transformed into carbon shell, resulting the carbon-coated Fe_3O_4 nanotubes. Such a hierarchical porous structure can buffer the volume changes during Li insertion/extraction.

Metallic carbonate compounds, which can generate CO_2 molecules during pyrolysis, can also be used as precursors to fabricate mesoporous metal oxide@carbon hybrids by using CNP strategy. Cheng et al. synthesized cubic mesoporous MnO@carbon hybrid composed of MnO nanoparticles in a porous carbon shell by using $MnCO_3$ as core and polydopamine as shell followed by pyrolysis process [58]. During pyrolysis, the CO_2 gases generated from carbonate decomposition *in situ* were gathered in the interior space owing to the polydopamine-encapsulated shell, which caused a high interior pressure to create homogeneous mesopores throughout the material due to the self-activation effect. To further extend the range of application promoted by this strategy, two other carbonates, $CoCO_3$ and $FeCO_3$, can also be chosen as precursors of metal oxide nanoparticles to fabricate mesoporous metal oxide@C hybrids with interior interlinked metal oxide nanoparticles and porous carbon shell.

4 Applications

The HSPCs fabricated through the CNP strategy feature exceptional dispersibility, fine-tuned cavity and highly developed porosity. Thus, they show great advantages in applications where call for special requirements in dispersion and confined reservoir, such as drug delivery, environment remediation, nanoreactor, etc.

4.1 HSPCs for drug delivery

Drug delivery is essential for future pharmaceutics, which relies on the development of novel nanocarriers for effective therapeutic delivery of drugs to targeted sites. Ideally, a nanocarrier material should have the following characteristics: (1) a high dispersion to allow nanocarriers with desirable blood circulation performance, (2) a high drug loading capacity to increase the nanocarrier's efficiency, (3) a high biocompatibility and structural stability to ensure a high biosafety used *in vivo* for a prolonged circulation time. The HSPCs prepared from the CNP strategy well meet these requirements, particularly in terms of excellent dispersibility, controlled nanocavity and high stability. For example, Wang et al. [59] designed hollow carbon spheres via CNP method which provide excellent drug loading capacity (1,350 $mg \cdot g^{-1}$) as compared with other carbonaceous nanocarriers [60, 61]. More importantly, the HSPCs exhibit excellent dispersion in aqueous solutions than other carbonaceous nanomaterials, which usually require additional dispersion promotor such as surfactants etc. [62, 63]. Benefiting from these properties, the HCSs were used to combat chemoresistance using synergistic chemo-therapy and laser irradiation stimuli to produce heat and free radicals (Fig. 14(a)).

In addition, the multi-functionalization of HSPCs derived from CNP strategy can be realized by combining carbon materials with functional nanoparticles (such as magnetic particles, etc.). For instance, a novel kind of highly dispersible HSPCs with a magnetic core was applied as MRI contrast agent due to its high paramagnetism of 90 $emu \cdot g^{-1}$ and also exhibit excellent photothermal effect of the HSPCs in the photothermal therapy (Fig. 14(b)) [25].

4.2 HSPCs for energy storage materials

From portable electronics to electric vehicles, energy storage devices play an important role in the development of these technologies. The realization of the function benefits from its charging and discharging mechanism. But in the process, insertion and extraction of ions (e.g., Na^+, K^+) cause uncontrollable volume expansion/contraction, which deteriorate the cycling performance. Therefore, it is particularly important to design a cushioned material to restrain its volume expansion. HSPCs

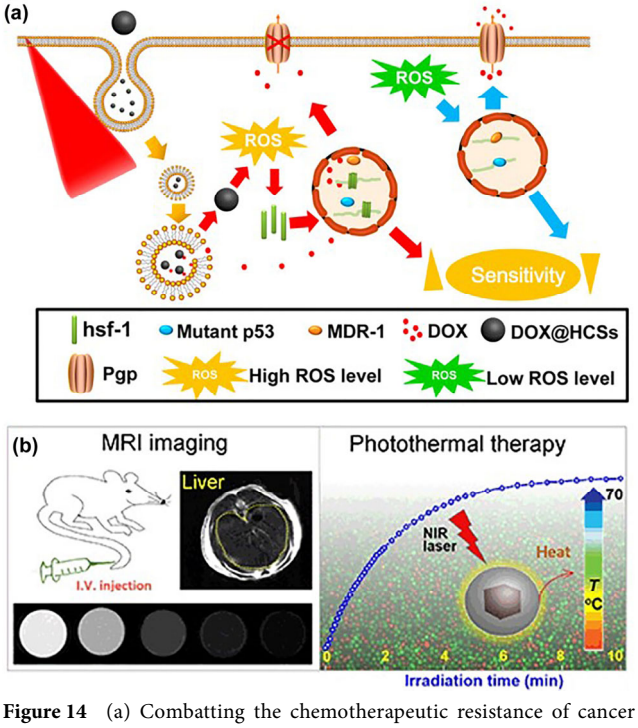

Figure 14 (a) Combatting the chemotherapeutic resistance of cancer using HCSs under NIR laser irradiation. (b) Schematic illustration of the application in MRI contrast agent and photothermal therapy. (a) Reproduced with permission from Ref. [59], © American Chemical Society 2015. (b) Reproduced with permission from Ref. [25], © Tsinghua University Press and Springer-Verlag Berlin Heidelberg 2016.

with tunable cavity is capable of providing buffer space for the huge volume variation upon charge and discharge. In lithium-sulfur batteries, the employing of hollow space can cushion the large volumetric variation (≈ 80%) between sulfur and Li_2S during the lithiation/delithiation process, which avoiding the reducing of the mechanical integrality and stability of sulfur cathode [64–69].

For lithium-ion or sodium-ion batteries, HSPCs also exhibit excellent potential. They may act as reservoirs to host active species, thus to buffer the huge volume variation during charging and discharging process. Silicon, one of the most abundant, geographically ubiquitous element, is regarded as the most promising anode materials for LIB due to the high theoretical specific capacity (≈ 4,200 $mAh·g^{-1}$, almost 11 times higher than capacity of graphite), low discharge voltage as anode, and low polarization capability. However, Si experiences an extreme volume expansion of 400% during a full lithiation process (up to $Li_{4.4}Si$), resulting in serious pulverization of the electrode and contact loss with the current collector in the first few cycles and leading to a rapid capacity decay. Fortunately, when silicon nanoparticles were confined in the cavity of HCSs, the carbon shell could provide finite inner voids for buffering the large volume changes of silicon nanoparticles, thus to enhance the cycling performance [70]. Moreover, this strategy is also suitable for various active species suffered from the same stability problems, including SiO_2, SnO_2, Mo, MoS_2, and $MoSe_2$, by anchoring them in the internal voids, inside the carbon walls, or on the out surface of the HCSs [71–73].

Overall, the CNP strategy, due to its strong cavity designability, can realize the nano-customization of cavities required by users, so it has extensive application potential in the field of energy storage and conversion.

4.3 HSPCs for nanoreactors

Nanoreactor, as the name implies, is a reactor at the nanoscale. Compared with the conventional reactors, nanoreactor can greatly simplify mass transfer, heat transfer and flow dynamics, which is beneficial to study the intrinsic kinetics of the chemical reactions more directly, and to establish the relationship between intrinsic dynamics and apparent dynamics. HSPCs, derived from CNP method, possess good dispersibility, available hollow space and porous carbon shell, are ideal for micro/nanoreactors because the cavity can concentrate reactants and store products, and the porous carbon shell can facilitate the loading of active species and avoid sintering during high-temperature reaction process. Nanoreactor can be used as model system to study the effect of microenvironment on chemical reactions. For example, Wang et al. fabricated PdCu embedded hollow carbon nanoreactors. The cavity can change the concentration and residence time of reactants in the microenvironment, and the selective regulation of reaction products can be realized by adjusting the spatial distribution of PdCu nanoparticles (Fig. 15(a)) [74]. Ma et al. [75, 76] fabricated a copper silicate nanoreactor with a nanotube-assembled hollow sphere (NAHS) to investigate the effect of morphology on the activity and selectivity in dimethyl oxalate (DMO) hydrogenation reaction (Fig. 15(b)) [75].

Taking the advantage of photothermal effect of carbon materials having broad photo-response in the range of 230–800 nm, covering ultraviolet and visible regions of sunlight, and the existence of cavities can increase the inverse range of light and greatly enhance the photothermal effect of carbon materials. Jiang and co-workers synthesized hollow porous carbons derived from PS@ZIF-8 [77]. Under 300 $mW·cm^{-2}$ full-spectrum light irradiation, the temperature of DMF solution

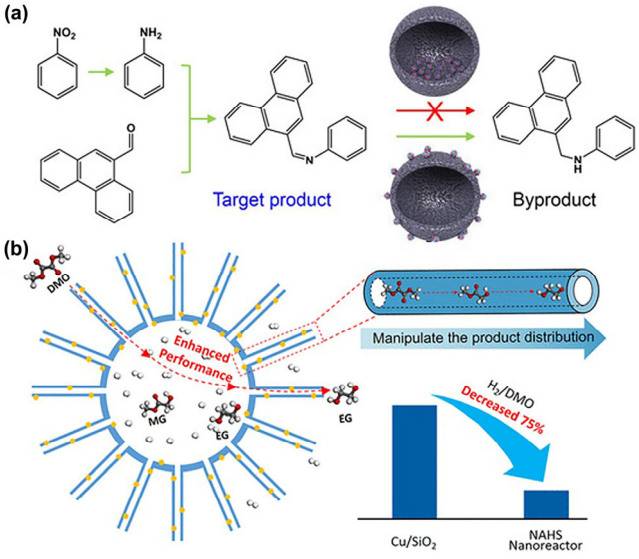

Figure 15 (a) Scheme of the cascade reductive coupling of nitroarene with a carbonyl compound over PdCu located interior or external of hollow carbon sphere. (b) Scheme of nanotube-assembled hollow sphere nanoreactor for DMO hydrogenation. (a) Reproduced with permission from Ref. [74], © The Authors. Published by Wiley-VCH GmbH 2020. (b) Reproduced with permission from Ref. [75], © The American Chemical Society 2019.

in the presence of N-doped porous carbon spheres rose from 20 to 65 °C. Benefiting from the excellent photothermal effect, the hollow porous carbons exhibited excellent performance in the CO_2 cycloaddition with epoxides under light irradiation at ambient temperature. The yield was extremely high (94%) compared with no light conditions (< 5%). In addition to adjustable cavities, excellent dispersibility in aqueous solution can increase the contact between active sites and reactants, thus achieving high catalytic performance. Therefore, CNP strategy has a broad application prospect in the design of nanoreactors.

4.4 HSPCs for environment remediation

Due to the self-activation process and confined space, CNP strategy is capable of producing carbon nanospheres with highly porous structure and discrete nanoparticles, which has a wide range of application value in water purification fields. An example is a novel kind of highly dispersible HSPCs prepared through the CNP strategy [16]. In addition to the excellent dispersibility, the HSPCs also shows a high specific surface area of 1,167 $m^2·g^{-1}$. Wang et al. developed an extended CNP strategy, in which a confined layer composed of silica nanoparticles by surface charge-driven interfacial assembly was employed. By doing so, a series of mesoporous HSPCs with rough surface was achieved. Such rough carbon nanospheres revealed a much higher adsorption rate and capacity over the direct-pyrolyzed carbon nanospheres for removing and recovering organic water pollutants (e.g., fluorescent derivatives) (Fig. 16) [26]. The difference in adsorption performance was attributed to the water dispersibility, surficial open mesopores, and appropriate surface roughness which could provide larger outer space to adsorb the fluorescent derivatives, leading to high adsorption capacity and faster adsorption rate.

Beside the organic water pollutants, the heavy-metal ions from polluted water have aroused increasing attention as a result of their nonbiodegradable nature and the tendency for accumulation in living organisms. Hollow carbon nanospheres with microporous shell and magnetic nanoparticles possess

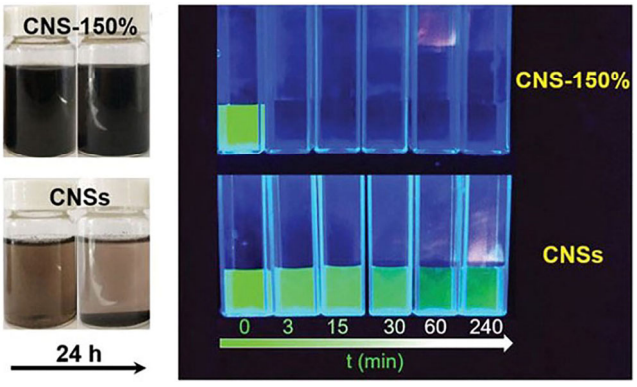

Figure 16 Dispersed solution of carbon nanospheres derived from surface-charge driven method and direct pyrolysis, and the time dependent removal of FITC from solutions. Reproduced with permission from Ref. [26]. © WILEY-VCH Verlag GmbH & Co. KGaA, Weinheim 2019.

high adsorption performance and magnetic separability for removal of chromium ions [10, 78]. Therefore, HSPCs synthesized by such CNP strategy can serve as ideal adsorbents for the removal and recovery of organic pollutants and heavy-metal ions from waste water.

5 Conclusion and perspective

Confined nanospace pyrolysis strategy emerges as a unique technology to prepare hollow nanocarbon structures with exceptional monodispersity and fine-tuned interior cavity and shell's porosity, which attracted much attention in diverse applications. In this review, we have summarized the latest development of the CNP strategy. A special focus has been placed on the unique merits of this strategy, including the inhibition of agglomeration during high-temperature pyrolysis to ensure excellent monodispersity, the self-activation mechanism to ensure the *in-situ* formation of inner cavity, the controllability of hollow structure and porosity by tuning the parameters of confinement degree as well as the universality on the extension from spherical to non-spherical and from polymers to other composite materials. The underlying mechanisms and principles have been fully discussed so as to provide theoretical guidance for the design and synthesis of application orientated functional hollow structured porous materials.

In view of HSPCs' applications, in various types of batteries, the available cavities and porous carbon walls can mitigate the volume changes during charge-discharge and host active species, which can greatly enhance the cycling performance and electrochemical catalytic activity. In the field of catalysis, HSPCs nanoreactor can enhance the mass transfer and heat transfer of the reactants, so as to boost the reactions. The morphology, cavity size and location of active sites can affect the microenvironments including the aggregation state of reactants or products and the concentration near the active sites. By adjusting these parameters of the nanoreactors, the activity and selectivity can be regulated intelligently, thus to improve the performance of nanocatalysts.

Despite the significant progresses of the CNP strategy, there are still several open questions requiring further efforts in future. The first issue is that in the synthesis process, shrinkage or even collapse of the cavity and pore structure may occur during the silica removal process. According to the cavity formation mechanism, the carbonaceous volatiles deposit in the pores of the silica shell and form the twin-like carbon/silicon hybrids. After etching silica, the remained carbon framework may not be strong enough to maintain the original hollow and porous structure, resulting in the shrinkage or even collapse. Thus, it is of importance to develop strategies to strengthen the carbon shell and maintain the structural stability in multi-step treatments. In addition, combining the CNP strategy with other synthesis techniques to fabricate multifunctional HSPCs would also be a promising direction for a tailored application.

Last but not least, the scalable synthesis based on the CNP strategy needs to be strengthened. The primary issue needs to solve is that the preparation of polymer spheres with uniform and controllable particle size distribution under large-scale production conditions. Particle size uniformity is greatly affected by mass transfer and heat transfer. Non-uniform mass transfer and heat transfer will cause uncontrolled reaction, thus leading to non-uniform particle sizes of the synthesized polymer spheres. Therefore, in future research, the design of appropriate reactors to ensure the largest reverse-mixing, ensuring a homogeneous mass and heat transfer is particularly important. All in all, considering the rapid development and important advances of the CNP strategy, we believe it would attract more interests in not only chemistry and materials field, but also for targeted applications where precisely tailored nanocarbon materials are required.

Acknowledgements

The research was financially supported by the National Natural Science Foundation of China (Nos. 20873014 and 21073026), National Natural Science Foundation for Distinguished Young Scholars (No. 21225312) and the Cheung Kong Scholars Program of China (No. T2015036).

References

[1] Bin, D. S.; Li, Y. M.; Sun, Y. G.; Duan, S. Y.; Lu, Y. X.; Ma, J. M.; Cao, A. M.; Hu, Y. S.; Wan, L. J. Structural engineering of multishelled hollow carbon nanostructures for high-performance Na-ion battery anode. *Adv. Energy Mater.* **2018**, *8*, 1800855.

[2] Liu, J.; Kopold, P.; Wu, C.; Van Aken, P. A.; Maier, J.; Yu, Y. Uniform yolk–shell Sn_4P_3@C nanospheres as high-capacity and cycle-stable anode materials for sodium-ion batteries. *Energy Environ. Sci.* **2015**, *8*, 3531–3538.

[3] Pei, F.; Lin, L. L.; Fu, A.; Mo, S. G.; Ou, D. H.; Fang, X. L.; Zheng, N. F. A two-dimensional porous carbon-modified separator for high-energy-density Li-S batteries. *Joule* **2018**, *2*, 323–336.

[4] Chen, C. H.; Wang, H. Y.; Han, C. L; Deng, J.; Wang, J.; Li, M. M.; Tang, M. H.; Jin, H. Y.; Wang, Y. Asymmetric flasklike hollow carbonaceous nanoparticles fabricated by the synergistic interaction between soft template and biomass. *J. Am. Chem. Soc.* **2017**, *139*, 2657–2663.

[5] Zhang, H. B.; Liu, Y. Y.; Chen, T.; Zhang, J. T.; Zhang, J.; Lou, X. W. D. Unveiling the activity origin of electrocatalytic oxygen evolution over isolated Ni atoms supported on a N-doped carbon matrix. *Adv. Mater.* **2019**, *31*, 1904548.

[6] Kim, S. Y.; Jeong, H. M.; Kwon, J. H.; Ock, I. W.; Suh, W. H.; Stucky, G. D.; Kang, J. K. Nickel oxide encapsulated nitrogen-rich carbon hollow spheres with multiporosity for high-performance pseudocapacitors having extremely robust cycle life. *Energy Environ. Sci.* **2015**, *8*, 188–194.

[7] Chen, W. H.; Qiao, R.; Song, C. S.; Zhao, L. H.; Jiang, Z. J.; Maiyalagan, T.; Jiang, Z. Q. Tailoring the thickness of $MoSe_2$ layer of the hierarchical double-shelled N-doped carbon@$MoSe_2$ hollow nanoboxes for efficient and stable hydrogen evolution reaction. *J. Catal.* **2020**, *381*, 363–373.

[8] Zhao, R. H.; Wang, H.; Gao, N.; Liu, R.; Guo, T. Y.; Wu, J. T.; Zhang, T.; Li, J. P.; Du, J. P.; Asefa, T. Hollow hemispherical carbon microspheres with Mo_2C nanoparticles synthesized by precursor design: Effective noble metal-free catalysts for dehydrogenation. *Small Methods* **2020**, *4*, 1900597.

[9] Yang, H.; Bradley, S. J.; Chan, A.; Waterhouse, G. I. N.; Nann, T.; Kruger, P. E.; Telfer, S. G. Catalytically active bimetallic nanoparticles supported on porous carbon capsules derived from metal–organic framework composites. *J. Am. Chem. Soc.* **2016**, *138*, 11872–11881.

[10] Liu, D. H.; Guo, Y.; Zhang, L. H.; Li, W. C.; Sun, T.; Lu, A. H. Switchable transport strategy to deposit active Fe/Fe_3C cores into hollow microporous carbons for efficient chromium removal. *Small* **2013**, *9*, 3852–3857.

[11] Chen, Y.; Xu, P. F.; Wu, M. Y.; Meng, Q. S.; Chen, H. R.; Shu, Z.; Wang, J.; Zhang, L. X.; Li, Y. P.; Shi, J. L. Colloidal RBC-shaped, hydrophilic, and hollow mesoporous carbon nanocapsules for highly efficient biomedical engineering. *Adv. Mater.* **2014**, *26*, 4294–4301.

[12] Zhang, J. F.; Zhang, J.; Li, W. Y.; Chen, R.; Zhang, Z. Y.; Zhang, W. J.; Tang, Y. B.; Chen, X. Y.; Liu, G.; Lee, C. S. Degradable hollow mesoporous silicon/carbon nanoparticles for photoacoustic imaging-guided highly effective chemo-thermal tumor therapy *in vitro* and *in vivo*. *Theranostics* **2017**, *7*, 3007–3020.

[13] Hofer, C. J.; Grass, R. N.; Zeltner, M.; Mora, C. A.; Krumeich, F.; Stark, W. J. Hollow carbon nanobubbles: Synthesis, chemical functionalization, and container-type behavior in water. *Angew. Chem., Int. Ed.* **2016**, *55*, 8761–8765.

[14] Chen, Y.; Chen, H. R.; Zeng, D. P.; Tian, Y. B.; Chen, F.; Feng, J. W.; Shi, J. L. Core/shell structured hollow mesoporous nanocapsules: A potential platform for simultaneous cell imaging and anticancer drug delivery. *ACS Nano* **2010**, *4*, 6001–6013.

[15] Zhang, S. J.; Qian, X. Q.; Zhang, L. L.; Peng, W. J.; Chen, Y. Composition–property relationships in multifunctional hollow mesoporous carbon nanosystems for pH-responsive magnetic resonance imaging and on-demand drug release. *Nanoscale* **2015**, *7*, 7632–7643.

[16] Lu, A. H.; Sun, T.; Li, W. C.; Sun, Q.; Han, F.; Liu, D. H.; Guo, Y. Synthesis of discrete and dispersible hollow carbon nanospheres with high uniformity by using confined nanospace pyrolysis. *Angew. Chem., Int. Ed.* **2011**, *50*, 11765–11768.

[17] Liu, J.; Qiao, S. Z.; Chen, J. S.; Lou, X. W. D.; Xing, X. R.; Lu, G. Q. Yolk/shell nanoparticles: New platforms for nanoreactors, drug delivery and lithium-ion batteries. *Chem. Commun.* **2011**, *47*, 12578–12591.

[18] Liu, T.; Zhang, L. Y.; Cheng, B.; Yu, J. G. Hollow carbon spheres and their hybrid nanomaterials in electrochemical energy storage. *Adv. Energy Mater.* **2019**, *9*, 1803900.

[19] Tian, H.; Liang, J.; Liu, J. Nanoengineering carbon spheres as nanoreactors for sustainable energy applications. *Adv. Mater.* **2019**, *31*, 1903886.

[20] Fu, A.; Wang, C. Z.; Pei, F.; Cui, J. Q.; Fang, X. L; Zheng, N. F. Recent advances in hollow porous carbon materials for Lithium–Sulfur batteries. *Small* **2019**, *15*, 1804786.

[21] Prieto, G.; Tüysüz, H.; Duyckaerts, N.; Knossalla, J.; Wang, G. H.; Schüth, F. Hollow nano-and microstructures as catalysts. *Chem. Rev.* **2016**, *116*, 14056–14119.

[22] Qiao, Z. A.; Guo, B. K.; Binder, A. J.; Chen, J. H.; Veith, G. M.; Dai, S. Controlled synthesis of mesoporous carbon nanostructures via a "silica-assisted" strategy. *Nano Lett.* **2013**, *13*, 207–212.

[23] Fuertes, A. B.; Valle-Vigón, P.; Sevilla, M. One-step synthesis of silica@resorcinol–formaldehyde spheres and their application for the fabrication of polymer and carbon capsules. *Chem. Commun.* **2012**, *48*, 6124–6126.

[24] Fang, X. L.; Zang, J.; Wang, X. L.; Zheng, M. S.; Zheng, N. F. A multiple coating route to hollow carbon spheres with foam-like shells and their applications in supercapacitor and confined catalysis. *J. Mater. Chem. A* **2014**, *2*, 6191–6197.

[25] Lu, A. H.; Zhang, X. Q.; Sun, Q.; Zhang, Y.; Song, Q. W.; Schüth, F.; Chen, C. Y.; Cheng, F. Precise synthesis of discrete and dispersible carbon-protected magnetic nanoparticles for efficient magnetic resonance imaging and photothermal therapy. *Nano Res.* **2016**, *9*, 1460–1469.

[26] Wang, Q. G.; He, L.; Zhao, L. Y.; Liu, R. S.; Zhang, W. P.; Lu, A. H. Surface charge-driven nanoengineering of monodisperse carbon nanospheres with tunable surface roughness. *Adv. Funct. Mater.* **2020**, *30*, 1906117.

[27] Sun, Q.; Li, W. C.; Lu, A. H. Insight into structure-dependent self-activation mechanism in a confined nanospace of core–shell nanocomposites. *Small* **2013**, *9*, 2086–2090.

[28] Yang, T. Y.; Liu, J.; Zhou, R. F.; Chen, Z. G.; Xu, H. Y.; Qiao, S. Z. Monteiro, M. J. N-doped mesoporous carbon spheres as the oxygen reduction reaction catalysts. *J. Mater. Chem. A* **2014**, *2*, 18139–18146.

[29] Du, J.; Yu, Y. F.; Liu, L.; Lv, H. J.; Chen, A. B.; Hou, S. L. Confined-space pyrolysis of polystyrene/polyacrylonitrile for Nitrogen-Doped hollow mesoporous carbon spheres with high supercapacitor performance. *ACS Appl. Energy Mater.* **2019**, *2*, 4402–4410.

[30] Du, J.; Liu, L.; Yu, Y. F.; Hu, Z. P.; Zhang, Y.; Liu, B. B.; Chen, A. B. Tuning confined nanospace for preparation of N-doped hollow carbon spheres for high performance supercapacitors. *ChemSusChem* **2019**, *12*, 303–309.

[31] Du, J.; Liu, L.; Liu, B. B.; Yu, Y. F.; Lv, H. J.; Chen, A. B. Encapsulation pyrolysis synchronous deposition for hollow carbon sphere with tunable textural properties. *Carbon* **2019**, *143*, 467–474.

[32] Wang, T.; Sun, Y.; Zhang, L. L.; Li, K. Q.; Yi, Y. K.; Song, S. Y.; Li, M. T.; Qiao, Z. A.; Dai, S. Space-confined polymerization: Controlled fabrication of nitrogen-doped polymer and carbon microspheres with refined hierarchical architectures. *Adv. Mater.* **2019**, *31*, 1807876.

[33] Zhang, L. H.; He, B.; Li, W. C.; Lu, A. H. Surface free energy-induced assembly to the synthesis of grid-like multicavity carbon spheres with high level in-cavity encapsulation for lithium–sulfur cathode. *Adv. Energy Mater.* **2017**, *7*, 1701518.

[34] Yu, X. F.; Li, W. C.; Hu, Y. R.; Ye, C. Y.; Lu, A. H. Sculpturing solid polymer spheres into internal gridded hollow carbon spheres under controlled pyrolysis micro-environment. *Nano Res.* **2021**, *14*, 1565–1573.

[35] Yang, T. Y.; Zhou, R. F.; Wang, D. W.; Jiang, S. P.; Yamauchi, Y.; Qiao, S. Z.; Monteiro, M. J.; Liu, J. Hierarchical mesoporous yolk–shell structured carbonaceous nanospheres for high performance electrochemical capacitive energy storage. *Chem. Commun.* **2015**, *51*, 2518–2521.

[36] Yang, T. Y.; Liu, J.; Zheng, Y.; Monteiro, M. J.; Qiao, S. Z. Facile Fabrication of core–shell-structured Ag@carbon and mesoporous yolk–shell-structured Ag@carbon@silica by an extended stöber method. *Chem.—Eur. J.* **2013**, *19*, 6942–6945.

[37] Sun, Q.; He, B.; Zhang, X. Q.; Lu, A. H. Engineering of hollow core–shell interlinked carbon spheres for highly stable lithium–sulfur batteries. *ACS Nano* **2015**, *9*, 8504–8513.

[38] Du, J.; Liu, L.; Yu, Y. F.; Lv, H. J.; Zhang, Y.; Chen, A. B. Confined pyrolysis for direct conversion of solid resin spheres into yolk–shell carbon spheres for supercapacitor. *J. Mater. Chem. A* **2019**, *7*, 1038–1044.

[39] Du, J.; Liu, L.; Yu, Y. F.; Qin, Y. M.; Wu, H. X.; Chen, A. B. A confined space pyrolysis strategy for controlling the structure of hollow mesoporous carbon spheres with high supercapacitor performance. *Nanoscale* **2019**, *11*, 4453–4462.

[40] Zhang, X. H.; Li, Y. A.; Cao, C. B. Facile one-pot synthesis of mesoporous hierarchically structured silica/carbon nanomaterials. *J. Mater. Chem.* **2012**, *22*, 13918–13921.

[41] Zhang, H. H.; He, H. N.; Luan, J. Y.; Huang, X. B.; Tang, Y. G.; Wang, H. Y. Adjusting the yolk–shell structure of carbon spheres to boost the capacitive K^+ storage ability. *J. Mater. Chem. A* **2018**, *6*, 23318–23325.

[42] Yu, X. Y.; Hu, H.; Wang, Y. W.; Chen, H. Y.; Lou, X. W. Ultrathin MoS_2 nanosheets supported on N-doped carbon nanoboxes with enhanced lithium storage and electrocatalytic properties. *Angew. Chem., Int. Ed.* **2015**, *54*, 7395–7398.

[43] He, J. R.; Luo, L.; Chen, Y. F.; Manthiram, A. Yolk–shelled C@Fe_3O_4 nanoboxes as efficient sulfur hosts for high-performance lithium–sulfur batteries. *Adv. Mater.* **2017**, *29*, 1702707.

[44] Yang, F. H.; Gao, H.; Hao, J. N.; Zhang, S. L.; Li, P.; Liu, Y. Q.; Chen, J.; Guo, Z. P. Yolk–shell structured FeP@C nanoboxes as advanced anode materials for rechargeable lithium-/potassium-ion batteries. *Adv. Funct. Mater.* **2019**, *29*, 1808291.

[45] Liu, Y.; Kou, W.; Li, X. C.; Huang, C. Q.; Shui, R. B.; He, G. H. Constructing patch-Ni-shelled Pt@Ni nanoparticles within confined nanoreactors for catalytic oxidation of insoluble polysulfides in Li-S batteries. *Small* **2019**, *15*, 1902431.

[46] Zhang, H. W.; Noonan, O.; Huang, X. D.; Yang, Y. N.; Xu, C.; Zhou, L.; Yu, C. Z. Surfactant-free assembly of mesoporous carbon hollow spheres with large tunable pore sizes. ACS Nano 2016, 10, 4579–4586.

[47] Zang, J.; An, T. H.; Dong, Y. J.; Fang, X. L.; Zheng, M. S.; Dong, Q. F.; Zheng, N. F. Hollow-in-hollow carbon spheres with hollow foam-like cores for lithium–sulfur batteries. *Nano Res*. **2015**, *8*, 2663–2675.
[48] Ye, J. C.; Zang, J.; Tian, Z. W.; Zheng, M. S.; Dong, Q. F. Sulfur and nitrogen co-doped hollow carbon spheres for sodium-ion batteries with superior cyclic and rate performance. *J. Mater. Chem. A* **2016**, *4*, 13223–13227.
[49] Du, J.; Liu, L.; Hu, Z. P.; Yu, Y. F.; Qin, Y. M.; Chen, A. B. Order Mesoporous carbon spheres with precise tunable large pore size by encapsulated self-activation strategy. *Adv. Funct. Mater*. **2018**, *28*, 1802332.
[50] Zhang, X. Q.; Lu, A. H.; Sun, Q.; Yu, X. F.; Chen, J. Y.; Li, W. C. Unconventional synthesis of large pore ordered mesoporous carbon nanospheres for ionic liquid-based supercapacitors. *ACS Appl. Energy Mater*. **2018**, *1*, 5999–6005.
[51] Zhang, X. Q.; Sun, Q.; Dong, W.; Li, D.; Lu, A. H.; Mu, J. Q.; Li, W. C. Synthesis of superior carbon nanofibers with large aspect ratio and tunable porosity for electrochemical energy storage. *J. Mater. Chem. A* **2013**, *1*, 9449–9455.
[52] Zhang, X. Q.; He, B.; Li, W. C.; Lu, A. H. Hollow carbon nanofibers with dynamic adjustable pore sizes and closed ends as hosts for high-rate lithium-sulfur battery cathodes. *Nano Res*. **2018**, *11*, 1238–1246.
[53] Liu, C.; Huang, X. D.; Wang, J.; Song, H.; Yang, Y. N.; Liu, Y.; Li, J. S.; Wang, L. J.; Yu, C. Z. Hollow mesoporous carbon nanocubes: Rigid-interface-induced outward contraction of metal-organic frameworks. *Adv. Funct. Mater*. **2018**, *28*, 1705253.
[54] Shang, L.; Yu, H. J.; Huang, X.; Bian, T.; Shi, R.; Zhao, Y. F.; Waterhouse, G. I. N.; Wu, L. Z.; Tung, C H.; Zhang, T. R. Well-dispersed ZIF-derived Co, N-co-doped carbon nanoframes through mesoporous-silica-protected calcination as efficient oxygen reduction electrocatalysts. *Adv. Mater*. **2016**, *28*, 1668–1674.
[55] Lei, C.; Han, F.; Sun, Q.; Li, W. C.; Lu, A. H. Confined nanospace pyrolysis for the fabrication of coaxial Fe_3O_4@C hollow particles with a penetrated mesochannel as a superior anode for Li-ion batteries. *Chem.—Eur. J*. **2014**, *20*, 139–145.
[56] Han, F.; Li, W. C.; Lei, C.; He, B.; Oshida, K.; Lu, A. H. Selective formation of carbon-coated, metastable amorphous $ZnSnO_3$ nanocubes containing mesopores for use as high-capacity lithium-ion battery. *Small* **2014**, *10*, 2637–2644.
[57] Han, F.; Ma, L. J.; Sun, Q.; Lei, C.; Lu, A. H. Rationally designed carbon-coated Fe_3O_4 coaxial nanotubes with hierarchical porosity as high-rate anodes for lithium ion batteries. *Nano Res*. **2014**, *7*, 1706–1717.
[58] Cheng, F.; Li, W. C.; Lu, A. H. Using confined carbonate crystals for the fabrication of nanosized metal oxide@carbon with superior lithium storage capacity. *J. Mater. Chem. A* **2016**, *4*, 15030–15035.
[59] Wang, L. M.; Sun, Q.; Wang, X.; Wen, T.; Yin, J. J.; Wang, P. Y.; Bai, R.; Zhang, X. Q.; Zhang, L. H.; Lu, A. H. et al. Using hollow carbon nanospheres as a light-induced free radical generator to overcome chemotherapy resistance. *J. Am. Chem. Soc*. **2015**, *137*, 1947–1955.
[60] Gu, J. L.; Su, S. S.; Li, Y. S.; He, Q. J.; Shi, J. L. Hydrophilic mesoporous carbon nanoparticles as carriers for sustained release of hydrophobic anti-cancer drugs. *Chem. Commun*. **2011**, *47*, 2101–2103.
[61] Huang, X.; Wu, S. S.; Du, X. Z. Gated mesoporous carbon nano-particles as drug delivery system for stimuli-responsive controlled release. *Carbon* **2016**, *101*, 135–142.
[62] Xue, Z. H.; Zhang, F.; Qin, D. D.; Wang, Y. L.; Zhang, J. X.; Liu, J.; Feng, Y. J.; Lu, X. Q. One-pot synthesis of silver nanoparticle catalysts supported on N-doped ordered mesoporous carbon and application in the detection of nitrobenzene. *Carbon* **2014**, *69*, 481–489.
[63] Tanaka, S.; Fujimoto, H.; Denayer, J. F. M.; Miyamoto, M.; Oumi, Y.; Miyake, Y. Surface modification of soft-templated ordered mesoporous carbon for electrochemical supercapacitors. *Micropor. Mesopor. Mater*. **2015**, *217*, 141–149.
[64] Jayaprakash, N.; Shen, J.; Moganty, S. S.; Corona, A.; Archer, L. A. Porous hollow carbon@sulfur composites for high-power lithium–sulfur batteries. *Angew. Chem., Int. Ed*. **2011**, *50*, 5904–5908.
[65] Zhang, B.; Qin, X.; Li, G. R.; Gao, X. P. Enhancement of long stability of sulfur cathode by encapsulating sulfur into micropores of carbon spheres. *Energy Environ. Sci*. **2010**, *3*, 1531–1537.
[66] Zhou, W. D.; Wang, C. M.; Zhang, Q. L.; Abruña, H. D.; He, Y.; Wang, J. W.; Mao, S. X.; Xiao, X. C. Tailoring pore size of nitrogen-doped hollow carbon nanospheres for confining sulfur in lithium–sulfur batteries. *Adv. Energy Mater*. **2015**, *5*, 1401752.
[67] Zhou, G. M.; Zhao, Y. B.; Manthiram, A. Dual-confined flexible sulfur cathodes encapsulated in nitrogen-doped double-shelled hollow carbon spheres and wrapped with graphene for Li–S batteries. *Adv. Energy Mater*. **2015**, *5*, 1402263.
[68] Zhou, W. D.; Xiao, X. C.; Cai, M.; Yang, L. Polydopamine-coated, nitrogen-doped, hollow carbon–sulfur double-layered core–shell structure for improving lithium–sulfur batteries. *Nano Lett*. **2014**, *14*, 5250–5256.
[69] Yin, L. C.; Liang, J.; Zhou, G. M.; Li, F.; Saito, R.; Cheng, H. M. Understanding the interactions between lithium polysulfides and N-doped graphene using density functional theory calculations. *Nano Energy* **2016**, *25*, 203–210.
[70] Yang, T. Y.; Liang, J.; Sultana, I.; Rahman, M. M.; Monteiro, M. J.; Chen, Y.; Shao, Z. P.; Silva, S. R. P.; Liu, J. Formation of hollow MoS_2/carbon microspheres for high capacity and high rate reversible alkali-ion storage. *J. Mater. Chem. A* **2018**, *6*, 8280–8288.
[71] An, W. L.; Fu, J. J.; Su, J. J.; Wang, L.; Peng, X.; Wu, K.; Chen, Q. Y.; Bi, Y. J.; Gao, B.; Zhang, X. M. Mesoporous hollow nanospheres consisting of carbon coated silica nanoparticles for robust lithium-ion battery anodes. *J. Power Sources* **2017**, *345*, 227–236.
[72] Liu, H.; Guo, H.; Liu, B. H.; Liang, M. F.; Lv, Z. L.; Adair, K. R.; Sun, X. L. Few-layer $MoSe_2$ nanosheets with expanded (002) planes confined in hollow carbon nanospheres for ultrahigh-performance Na-ion batteries. *Adv. Funct. Mater*. **2018**, *28*, 1707480.
[73] Wang, J. J.; Luo, C.; Gao, T.; Langrock, A.; Mignerey, A. C.; Wang, C. S. An advanced MoS_2/carbon anode for high-performance sodium-ion batteries. *Small* **2015**, *11*, 473–481.
[74] Dong, C.; Yu, Q.; Ye, R. P.; Su, P. P.; Liu, J.; Wang, G. H. Hollow carbon sphere nanoreactors loaded with PdCu nanoparticles: Void-confinement effects in liquid-phase hydrogenations. *Angew. Chem., Int. Ed*. **2020**, *132*, 18532–18537.
[75] Yao, D. W.; Wang, Y.; Li, Y.; Zhao, Y. J.; Lv, J.; Ma, X. B. A high-performance nanoreactor for carbon–oxygen bond hydrogenation reactions achieved by the morphology of nanotube-assembled hollow spheres. *ACS Catal*. **2018**, *8*, 1218–1226.
[76] Yao, D. W.; Wang, Y.; Hassan-Legault, K.; Li, A. T.; Zhao, Y. J.; Lv, J.; Huang, S. Y.; Ma, X. B. Balancing effect between adsorption and diffusion on catalytic performance inside hollow nanostructured catalyst. *ACS Catal*. **2019**, *9*, 2969–2976.
[77] Yang, Q. H.; Yang, C. C.; Lin, C. H.; Jiang, H. L. Metal-organic-framework-derived hollow N-doped porous carbon with ultrahigh concentrations of single Zn atoms for efficient carbon dioxide conversion. *Angew. Chem., Int. Ed*. **2019**, *58*, 3511–3515
[78] Zhang, L. H.; Sun, Q.; Liu, D. H.; Lu, A. H. Magnetic hollow carbon nanospheres for removal of chromium ions. *J. Mater. Chem. A* **2013**, *1*, 9477–9483.